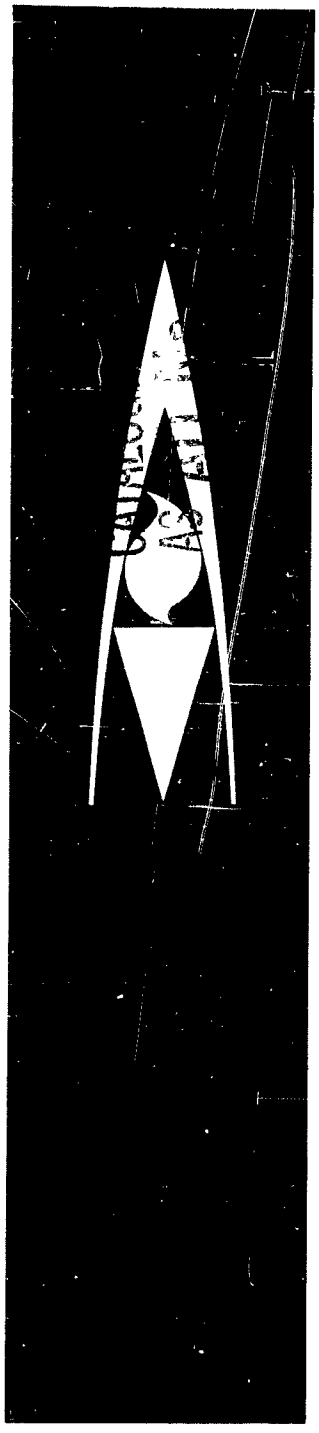

IMPROVEMENT OF THE USEFULNESS OF PYROLYTIC GRAPHITE IN ROCKET MOTOR APPLICATIONS

Final Technical Summary Report

BY
JAMES D. BATCHELOR
EDWIN F. FORD
EUGENE L. OLCOTT

February, 1963

Contract No. DA-36-034-ORD-3279Z Project No. TB 4-004

Atlantic Research Corporation
Alexandria, Virginia

ATLANTIC RESEARCH
CORPORATION

ATLANTIC RESEARCH CORPORATION
ALEXANDRIA, VIRGINIA

IMPROVEMENT OF THE USEFULNESS OF PYROLYTIC GRAPHITE IN ROCKET MOTOR APPLICATIONS

Final Technical Summary Report

Contract No. DA-36-034-ORD-3279 Z
Project No. TB 4-004

BY
JAMES D. BATCHELOR
EDWIN F. FORD
EUGENE L. OLCOTT

FEBRUARY, 1963

Atlantic Research Corporation
Alexandria, Virginia

ABSTRACT

This research program consisted of a systematic study of the utility of pyrolytic graphite for service in uncooled nozzles for solid propellant rocket motors. In an effort to improve the usefulness of pyrolytic graphite, studies were carried out in three areas. First, the effect of the deposition process conditions on the nature of the pyrolytic graphite coating formed was investigated. The pyrolytic graphite was characterized by density measurements, X-ray diffraction analysis, and microstructure examination. The deposition process was found sensitive to carbonaceous source gas concentration and local gas flow conditions with a lesser effect of temperature above about 1900°C. Little effect of the type of source gas was noted. Below about 1900°C the deposits became increasingly coarse with decreased temperature. Of several substrate surface preparations and pretreatments only a resin precoat seemed to hold promise of improving the microstructure of lower temperature coatings.

The second area of study was mechanical design analysis to assure that good design practice was utilized. The basic stress-strain relationships were derived for an anisotropic material such as pyrolytic graphite. The shear stresses in a coated system were also examined. The segmented nozzle design utilized throughout the successful motor firing studies was found to meet the requirements of good design.

The third major area of study consisted of the experimental measurement in sub-scale rocket nozzle tests of the inherent erosion rate of a standard (2000°C) pyrolytic graphite under a variety of motor operating conditions. Tests were made with propellants having flame temperatures from 5600°F to 6500°F and a range of oxidation ratios. For a given propellant the erosion rate was a function of the motor operating pressure. Over the range studied, propellant flame temperature was found more significant than oxidation ratio in determining the erosion rate. The performance of pyrolytic graphite coatings were excellent in all propellants at all motor pressures. Scale up from one-half inch test nozzles to a one inch diameter nozzle was successfully accomplished and proved in full duration, high pressure motor test. A two inch nozzle was designed and successfully fabricated prior to expiration of the contract funds.

FOREWORD

The research described in this report was sponsored by the U. S. Army under Contract DA-36-034-ORD-3279(Z). This contract was administered by the Ordnance Materials Research Office, Watertown Arsenal, Watertown, Massachusetts. Technical direction was provided by Mr. Charles H. Martens of the Propulsion Laboratory, Army Missile Command, Redstone Arsenal, Alabama. The work was carried out at the Atlantic Research Corporation principal laboratories, Alexandria, Virginia under the supervision of Mr. E. L. Olcott, Director of the Materials Division. The project director at Atlantic Research was Dr. James D. Batchelor with the able support of Messrs. E. F. Ford, S. W. McCormick, R. A. Davis, S. W. Miller, and R. K. White. The experimental work was performed over the period from June 1, 1960 through December 31, 1962.

TABLE OF CONTENTS

TABLE OF CONTENTS (Cont'd)

LIST OF FIGURES

LIST OF FIGURES (Cont'd)

LIST OF TABLES

I. INTRODUCTION

As rocket technology advances, the requirements for materials become more stringent. In solid-propellant rocket motors, uncooled hot parts are needed to maintain the inherent simplicity of the design. In the nozzle area the service conditions are extremely severe. High heat flux is combined with high erosion forces at the throat of the nozzle. Yet the maximum dimensional stability is required in this area to maintain the ballistic design performance of the motor.

Recent improvements in performance of solid propellants have been accompanied by increasingly severe operating conditions for rocket motor nozzles. High performance solid propellant formulations very often have flame temperatures of 6000°F or higher. Propellant flame temperatures of 6500-6600°F are not uncommon. These very high flame temperatures are accompanied in many cases by oxidation ratios substantially above unity, which leads to substantial quantities of such oxidizers as carbon dioxide and water vapor in the combustion products.

The effect of these severe environmental factors in solid propellant motors has resulted in the elimination of many refractory materials as candidates for nozzle service. A special form of carbon, produced by vapor deposition at high temperature and known generally as pyrolytic graphite, has certain inherent properties which immediately suggest merit as an uncooled nozzle for advanced solid-propellant rocket motors. The high sublimation temperature of carbon is well known. The strength of commercial graphite increases with temperature and at 4500°F is the highest of any known material. Graphite is extremely stable at high temperatures, being moderately sensitive only to oxidation. Pyrolytic graphite shares all of these desirable properties with other forms of graphite. In addition, this vapor-deposited form of graphite offers very high purity, extremely low porosity (high density), and highly oriented crystalline structure. Because of these desirable properties, pyrolytic graphite is an excellent candidate for rocket nozzle service.

The orientation of the crystallites in a pyrolytic graphite coating is such that the layer planes in the structure lie parallel to the substrate surface. Highly anisotropic thermal and mechanical properties result from this oriented structure. Pyrolytic graphite is an excellent conductor of heat along its surface and at the same time is a good insulator across its thickness. This combination of thermal properties can be advantageous in a rocket nozzle application, but the anisotropic mechanical properties that also exist can cause problems. The thermal expansion coefficients of pyrolytic graphite are large across its layer planes but very low along the layer plane. Since these expansion coefficients are not matched by commercial graphites usually used as substrates, stresses produced in the manufacture of pyrolytic graphite and stresses produced in service can cause fracture problems which must be overcome.

In the past, failures have been experienced in hasty applications of pyrolytic graphite in rocket nozzles; only a balanced study, in which the limitations as well as the desirable properties of pyrolytic graphite were a careful research program was required to determine the utility of pyrolytic graphite as a practical nozzle material. This report documents such a program in which the excellent performance capabilities of pyrolytic graphite were demonstrated in nozzle tests under severe motor operating conditions with nozzle throat diameters up to one inch.

II. SCOPE OF PROGRAM

The purpose of this program, as indicated by the title, was to study means to improve the usefulness of pyrolytic graphite for practical applications under critical service conditions in solid-propellant rocket motors. The scope of our program included the experimental study of the deposition process, analytical and experimental study of the mechanical design of pyrolytic graphite nozzles, the evaluation of pyrolytic graphite in rocket motor test firings, and the correlation of performance with those factors which determine it.

Although the desirability of several of the known properties of pyrolytic graphite was known, the effect of the deposition process conditions on those properties important for serviceability in a rocket nozzle was not well understood. The first phase of this program, therefore, involved the characterization of pyrolytic graphite deposited under a variety of conditions. In the first annual report on this program, the relation between the deposition process conditions and a number of characterization parameters was reported in some detail. It was found that a reasonably fine-grained pyrolytic graphite could be formed reproducibly from a methane-argon source gas mixture with a substrate temperature of 2000°C. The coatings formed under these conditions appeared to be of good quality and were selected for initial rocket motor nozzle tests.

Although several areas of interest were apparent for further study, two decisions affecting the principal emphasis of this program were made near the beginning of the second year's effort in discussions with the Ordnance Materials Research Office sponsors. First, it was agreed that a major emphasis would be placed on the preparation and test firing of sub-scale nozzles with pyrolytic graphite coatings. Work on the study of deposition process conditions and on mechanical design and stress analysis were to be pursued as a direct adjunct to the nozzle test program to improve reliability in the motor firings. The second decision was that the principal interest lay in the reliable measurement of the serviceability in nozzles of a good, standard grade of pyrolytic graphite. Quantitative performance data for this standard pyrolytic graphite under a variety of motor operating conditions, using a variety of typical propellants, were felt to be more important than the final optimization of the quality of the pyrolytic graphite deposit. Again, mechanical design analyses were considered desirable primarily to make certain that the performance data were not compromised by poor or inadequate design. A corollary benefit could

be anticipated in terms of background information useful in the scaling-up of nozzle designs from sub-scale to full-scale applications. The deposition process studies were oriented toward the discovery of substantially simpler or more effective processes for the preparation of pyrolytic graphite, rather than towards detailed or marginal improvements on the standard pyrolytic graphite grade.

Consistent with these decisions on the emphasis to be placed on different areas of research the program was carried out as follows. The first year was spent largely on a study of the deposition process and characterization of the pyrolytic graphite coatings produced under various process conditions. Preliminary motor testing and mechanical design analysis were initiated. During the next fifteen months major emphasis was placed on the preparation and motor testing of nozzles of nominal one-half inch diameter coated with a standard (2000°C) grade of pyrolytic graphite. Support work was carried out consisting of stress analyses for coatings and deposition studies aimed at simpler or more effective coating techniques. The final four months of the program was spent in scaling up motor tests to include firings with one inch diameter nozzles and preparation for two-inch nozzle tests.

III. DEFINITION OF TERMS

Graphite is a common term that is often used inaccurately. The term graphite has been applied at one time or another to almost every carbonaceous material which has been heat-treated at a high temperature. In the interest of clarity, more precise definitions are offered here for three terms which will be used repeatedly in this report. Although these definitions may not be the only acceptable ones, their statement here should improve the clarity of this report.

Graphite: An allotropic crystalline form of carbon. Used in this sense, the term graphite refers specifically to an ideal crystal structure: a stacked, hexagonal layer plane structure with 1.42 Å between carbon atoms forming regular hexagons in the layers and with a stacking distance of 3.354 Å between adjacent layer planes. Further, a complete three-dimensional order exists with an a-b-a arrangement of layer planes, i.e., the carbon atoms in alternate layer planes lie one above the other, while in intermediate layer planes a carbon atom lies over the center of the hexagon below it. The bonding in the layer planes (the a-direction) is by valence bonds, while the cross-layer bonding (the c-direction) is much weaker (largely Van der Walls type). The anisotropy of the properties of such a structure can be anticipated.

Commercial Graphite: A compact consisting of ground coke particles with a carbonized pitch binder. This term is perhaps the most difficult to define because it is applied to the greatest variety of materials. The degree of graphitization, i.e., the amount of carbon which has been converted to a highly structured form approaching the true graphite crystal, is established by the complete history of all ingredients in the material. Other things equal, the higher the baking temperature the further advanced is the graphitization. The anisotropy of a commercial graphite is determined both by the graphitizing thermal treatment which it has received and by the mechanical compaction it undergoes. Molded commercial graphite has some preferred orientation of the layer planes (a-axis) perpendicular to the pressing direction; extruded commercial graphite has some preferred orientation of the a-axis parallel to the extrusion axis. In general, the orientation of the particles and the resulting anisotropy of thermal and mechanical properties is not pronounced in commercial graphite. Current work on special hot-worked high-density grades of commercial graphite has produced higher than usual degrees of anisotropy.

Since the nature of a commercial graphite is determined by such a variety of factors--the source and nature of the granular coke, the source and nature of the binder pitch, the method and pressure of compaction, and the thermal treatment of the compact--the term must, at best, remain rather broad.

Pyrolytic Graphite: A form of carbon prepared by vapor deposition on a hot substrate and having a high degree of crystalline orientation. Since this material is built up on a hot surface, essentially atom by atom from a carbonaceous source gas, the orientation of the graphite layer planes is parallel to the substrate surface. In general, no orderly relation exists among the parallel stack of layer planes to yield a third-dimensional order. This so-called "turbostratic" structure, which is accompanied by a layer-stacking distance enlarged to about 3.44 Å, produces a marked degree of anisotropy in thermal and mechanical properties. Other characteristics of pyrolytic graphite include high purity and high density, approaching true density (zero porosity). The anisotropy, density, and purity will vary, of course, with the deposition conditions, but each is characteristically high. By analogy, pyrolytic graphite corresponds to a crystalline body solidified from a melt, while commercial graphite corresponds to a pressed and sintered, or briquetted body.

IV. LABORATORY STUDIES

A. DEPOSITION TECHNIQUE

Pyrolytic graphite is deposited by passing a carbonaceous source gas over a hot substrate. Substrate temperatures in the range of 1600°C to 2400°C are generally required. In the work reported herein, heating of the substrate was accomplished by placing the substrate tube along the axis of a 4-inch diameter resistance-heated tube furnace (Pereny Equipment Company, Model C412). This furnace, which has a 4-foot heated length, can maintain controlled temperatures from 1300°C to 3000°C using a magnetic amplifier-saturable reactor control system. The sensing element is a radiometer which is focused on the outer surface of the substrate tube through a sight tube at the center of the furnace. Two views of this furnace, its associated temperature control unit, and the gas flow control equipment are shown in Figures 1 and 2.

The source gas which was controlled with standard rotameters, was taken from commercial compressed gas cylinders. Carbonaceous source gases used included methane, propane, acetylene, and ethylene. The inert gas used as a diluent in the process stream and for protection of the furnace heating element throughout the program was argon. All the deposition tests were made at atmospheric pressure with the process gases discharging directly into the ventilation hood placed above the end of the furnace.

Each of the deposition runs made in the process studies used a 1-inch inside diameter by 1-1/2 inch outside diameter graphite tube as the substrate. In the first six runs, the process gas mixture of methane and argon entered the substrate tube outside the heated zone of the furnace and passed through the substrate tube for the entire length of the heated section. With this technique the pyrolytic graphite deposit was formed wherever the substrate temperature was high enough to promote deposition. Temperature measurements taken by sighting an optical pyrometer on the face of a thin graphite disc placed at various stations along the length of the heated tube indicated that a substantial temperature gradient existed near each end of the furnace. However, within a 12-inch section centered in the furnace the temperature was essentially uniform. Therefore, the deposition procedure was

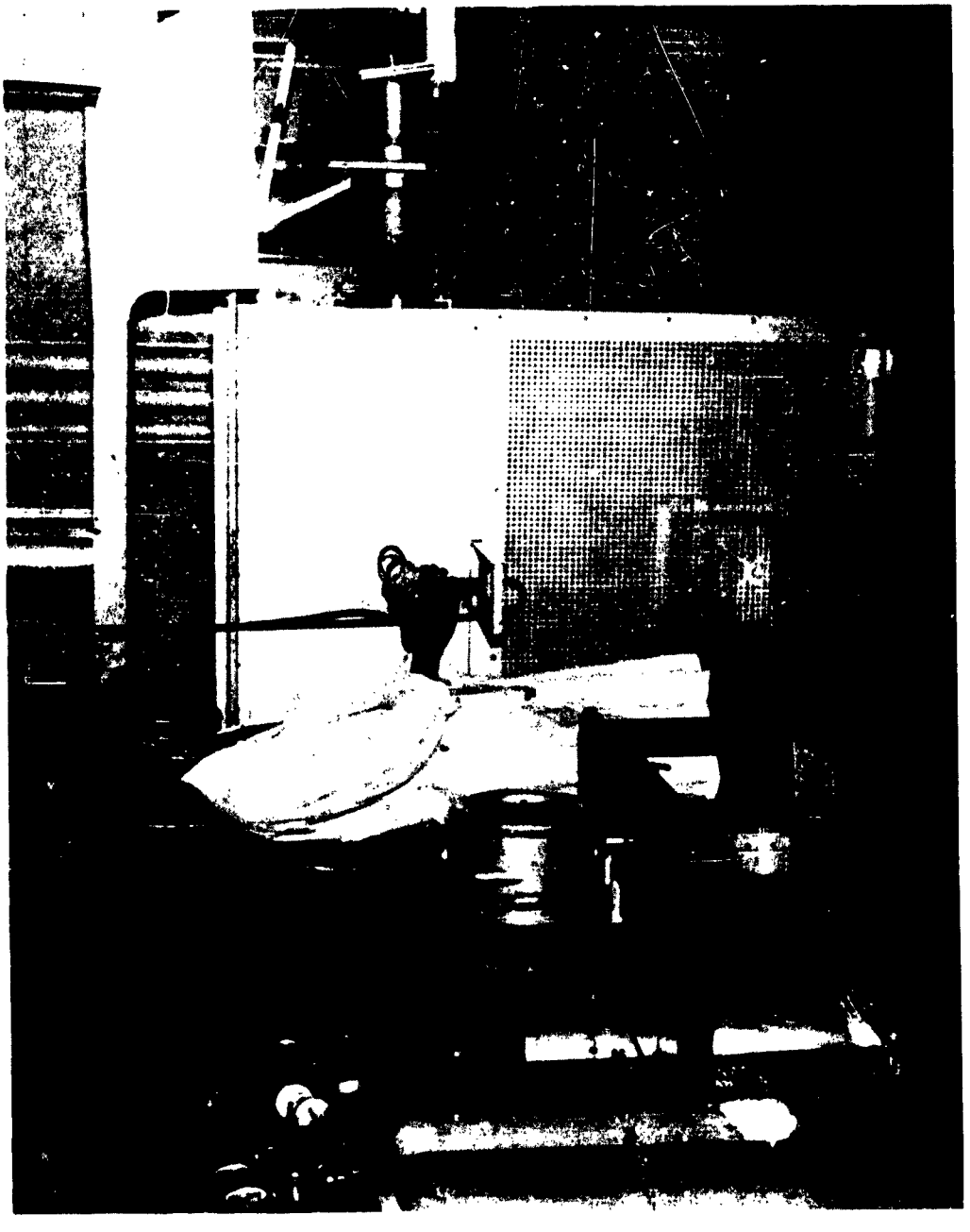

Figure 1. Pyrolytic Graphite Deposition Furnace.

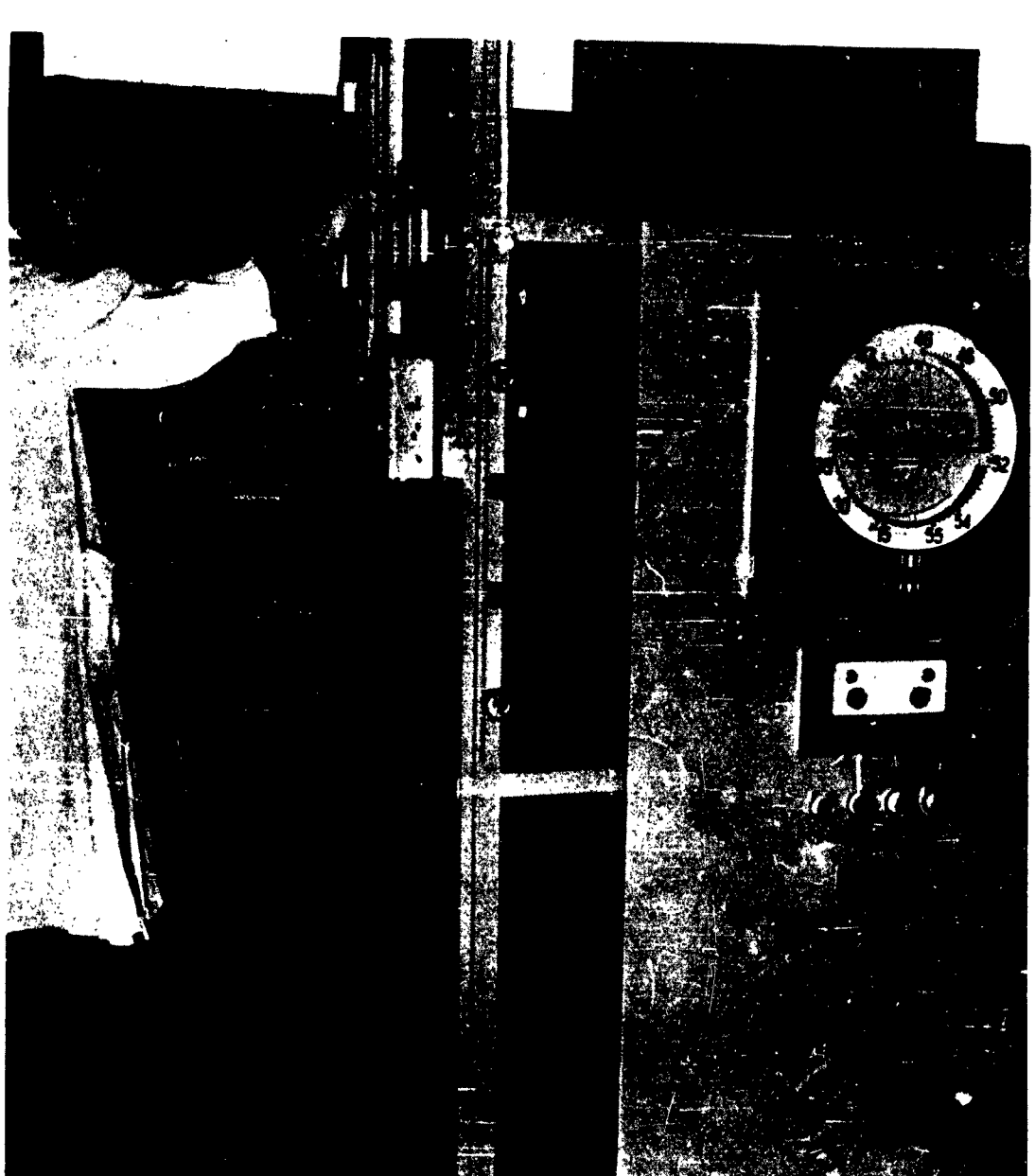

Figure 2. Pyrolytic Graphite Furnace Controls.

changed to place a 12-inch test section of the substrate at the center of the furnace tube. Starting with Run 7 the substrate tube consisted of an inlet section, a 12-inch test section, and an outlet section joined by sleeve couplings. The over-all substrate assembly (approximately 6 feet long) was placed so that the 12-inch test section lay at the center of the furnace. Since the inlet and outlet section were reusable, only the test section was removed for examination following each deposition run. To initiate the deposition at the inlet of the test section, a water-cooled injector was used to transport the source gas to this point. The injector consists of three concentric tubes; gas passes through the inner tube, water enters through the middle tube, and water leaves through the outer tube. A replaceable, uncooled graphite nozzle can be threaded onto the outlet end of the injector. The carbonaceous source gas always flows through the injector; the inert argon diluent gas can be split with part of the flow going through the injector and part outside the injector. The gas dynamics and the temperature of the combined process gas at the injector outlet can be changed by varying the proportion of the argon which enters through the annulus outside the injector where it is subject to preheating.

B. CHARACTERIZATION METHODS

Following each deposition run, the 12-inch test section was split length-wise (top to bottom) to expose the pyrolytic graphite coating. A measurement was made of the thickness of the deposit at one inch intervals along the substrate length at both the top and bottom; these measurements were made with a low-power microscope with a calibrated eye-piece scale. One half-section of the substrate was then further cut into six sections 2-inches long; these sections are numbered one to six from the inlet end. Each section was polished for microscopic examination. When needed powder samples were scraped from these sections for X-ray and density measurements. The sample designation used lists the run number first and then the section number.

The methods used for the other characterization work are described in the following sections.

1. X-Ray Diffraction Analysis

North American Philips X-ray Diffraction Equipment was used to determine interplanar spacings, crystallite dimensions, and relative peak intensities for pyrolytic graphite samples. X-ray diffraction patterns were obtained using Cobalt Kα radiation and standard X-ray procedures. Sodium chloride was used as an external standard to determine instrumental line broadening. Exploratory tests were made using admixtures of NaCl and graphite; but because of the possibility of peak interference and sample contamination, all NaCl patterns were determined separately. The 2θ position of the pure sodium chloride peaks also served as a check against instrumentation error.

Interplanar spacings (d-spacings) of the basal planes in the pyrolytic graphite were calculated using Bragg's Law. The crystallite dimensions L_c and L_a were determined from the line broadening of selected reflections at half-maximum intensity. L_c represents the average crystallite dimension in the stacking direction; L_a represents the average crystallite diameter on the basal planes. Both parameters were calculated by Scherrer's equation using Warren's technique for correcting for instrumental line broadening.

The peaks selected to determine the parameters L_c and L_a were the crystalline reflections of the 004 planes and the 10 bands, respectively. The 004 reflection is a typical symmetrical diffraction peak resulting from the uniform stacking of the layer planes. However, the 10 reflection rises sharply to a peak and then subsides slowly on the high angle side; this peak is caused by two-dimensional order in the graphite layer planes which produces a grating effect. If the turbostratic structure were to form a true graphitic 3-dimensional order, sharp peaks would be resolved from the 10 band. Conversely, the substantial absence of this resolution in the 10 band indicates a turbostratic structure.

2. Density

Density of the deposited material was determined by a sink-float technique using a mixture of bromoform and ethyl alcohol. The method consisted of placing the sample in a small beaker containing the liquid mixture. The density (composition) of the liquid mixture was then adjusted until the sample would neither sink nor float. Equilibrium was generally reached within 30 minutes. The density of the pyrolytic graphite was then equal to that of the liquid which was determined by weighing a known volume of the liquid.

3. Microstructure

Microstructural examinations were conducted on polished sections of the deposited material using a Zeiss metallurgical microscope and conventional techniques of microscopy. Sample preparation consisted of cross-sectioning the coating and substrate in a longitudinal direction and polishing on standard laps until smooth. Structural variations are readily distinguishable at moderate magnifications, such as 50X to 100X. Polarized light is desirable for studying the cone structure, a typical type of microstructure for most vapor-deposited materials. Improved polished sections were obtained by potting the sample in an epoxy resin before polishing. However, the polishing without resin potting was acceptable for the routine observation.

C. RESULTS FROM BASIC PROCESS STUDIES

During the first year of this program twenty-three deposition runs were made to investigate the effect of basic process conditions on the deposition of pyrolytic graphite. Coatings suitable for extensive characterization study were obtained in twenty of these runs. The conditions for each of these runs are given in Table I. Data on the pyrolytic graphite formed are listed in Table II. The first six runs were exploratory ones in which the equipment and deposition techniques were tested and improved. The remaining deposition runs were isothermal tests in which the effects of process conditions were studied.

The objective of these runs was to study the basic factors in pyrolytic graphite deposition such as temperature, gas concentration, and the like. Extensive examination of the coatings was carried out to provide background knowledge for later process improvements.

TABLE I

Operating Conditions in Basic Process Studies

Run No.	Carbonaceous Gas Concentration (per cent)	Per Cent of Gas* Through Injector	Deposition Temperature (°C)	Time (Hours)	Nozzle
(a) Exploratory, Non-Isothermal Runs					
2	5 CH_4	No Injector	1500 - 1950	2	
3	20 CH_4	No Injector	1500 - 1950	2	
4	5 CH_4	No Injector	1500 - 1950	2	
5	5 CH_4	No Injector	1650 - 2150	2	
6	10 CH_4	No Injector	1650 - 2150	2	
(b) Isothermal Deposition Runs					
7	14 CH_4	60	2000	2	None
8	6 CH_4	60	2000	2	None
9	6 CH_4	60	2200	2	None
10	6 CH_4	60	2100	2	None
12	2.5 CH_4	60	2000	3	None
13	5 CH_4	80	2000	4	Long
14	5 CH_4	90	2000	2	Long
15	2.5 CH_4	90	2000	4	Long
16	2.5 CH_4	90	1900	3	Long
17	2.5 C_3H_8	90	2000	2	Short
18	5 C_3H_8	90	2000	2	Short
19	2.5 C_3H_8	90	2000	2	Short
20	1.2 C_3H_8	90	2200	4	Short
22	5 CH_4	90	2400	3	Short
23	2.5 CH_4	90	2400	4	Short

* Total gas flow rate was 20 SCFH in all runs except Run 13 in which 10 SCFH was used.

TABLE II

Summary of Characterization Data on Pyrolytic Graphite

Sample No.*	Thickness (mils)	Density (gms/cc)	Crystallite Dimensions (Å)		004 Peak Intensity (Relative Units)
			L_a	L_c	
Run 2 (Inlet CH_4 Concentration = 6 Per Cent; Temperature = 1500 - 1950°C)					
2-2	14	--	83	40	
2-3	15	--	96	69	
2-4	13	--	112	69	
2-5	10	--	155	96	
2-6	7	--	106	75	
Run 3 (Inlet CH_4 Concentration = 25 Per Cent; Temperature = 1500 - 1950°C)					
3-2	22	--	70	46	
3-3	28	--	96	65	
3-4	34	--	118	76	
3-5	20	--	118	64	
3-6	14	--	165	79	
			121	91	
Run 4 (Inlet CH_4 Concentration = 6 Per Cent; Temperature = 1500 - 1950°C)					
4-2	16	1.88	84	45	
4-3	17	2.10	88	52	
4-4	13	2.06	106	80	
4-5	10	2.12	122	84	
4-6	8	2.12	125	82	
Run 5 (Inlet CH_4 Concentration = 6 Per Cent; Temperature = 1650 - 2150°C)					
5-1	14	1.85	88	47	
5-2	16	2.08	92	61	
5-3	14	2.09	143	83	
5-4	10	2.10	112	86	
5-5	5	2.13	92	93	
5-6	4	2.12	106	86	
Run 6 (Inlet CH_4 Concentration = 14 Per Cent; Temperature = 1650 - 2150°C)					
6-1	17	1.82	84	43	
6-2	29	1.96	88	57	
6-3	19	2.12	88	74	
6-4	16	2.21	96	82	
6-5	8	2.21	101	86	
6-6	4	2.22	81	74	

TABLE II (continued)

Sample No.*	Thickness (mils)	Density (gms/cc)	Crystallite Dimensions (Å) L_a	Crystallite Dimensions (Å) L_c	004 Peak Intensity (Relative Units)
Run 7 (Inlet CH_4 Concentration = 14 Per Cent; Temperature = 2000°C)					
7-1	8	2.18	101	83	
7-2	38	2.08	84	61	
7-3	39	2.19	84	69	
7-4	24	2.25	106	81	
7-5	Rough Coating	2.20	102	86	
7-6	Rough Coating	2.17	70	95	
Run 8 (Inlet CH_4 Concentration = 6 Per Cent; Temperature = 2000°C)					
8-1	5	2.21	81	--	
8-2	22	2.24	119	95	
8-3	24	2.22	92	68	
8-4	18	2.16	102	69	
8-5	13	2.22	143	74	
Run 9 (Inlet CH_4 Concentration = 6 Per Cent; Temperature = 2200°C)					
9-2	31	2.18	117	78	15.5
9-3	28	2.16	110	78	13.0
9-4	18	2.19	165	78	17.2
9-5	12	2.20	180	92	18.5
9-6	6	2.18	95	92	18.0
Run 10 (Inlet CH_4 Concentration = 6 Per Cent; Temperature = 2100°C)					
10-1	12	2.19	--	78	9.0
10-2	33	2.18	152	73	8.3
10-3	26	2.16	125	78	10.6
10-4	18	2.17	141	85	8.6
10-5	10	2.18	141	78	13.2
10-6	6	2.13	152	85	17.4
Run 12 (Inlet CH_4 Concentration = 2.5 Per Cent; Temperature = 2000°C)					
12-1	9	2.18	124	64	6.0
12-2	10	2.16	133	64	7.0
12-3	11	2.15	142	92	10.0
12-4	14	2.14	100	85	11.3
12-5	16	2.15	124	85	11.5
12-6	12	2.16	142	85	13.5

TABLE II (continued)

Sample No.*	Thickness (mils)	Density (gms/cc)	Crystallite Dimensions (Å) L_a	Crystallite Dimensions (Å) L_c	004 Peak Intensity (Relative Units)
Run 13 (Inlet CH_4 Concentration = 5 Per Cent; Temperature = 2000°C)					
13-1	15	2.13	132	78	6.0
13-2	20	2.17	179	92	7.5
13-3	18	2.15	143	78	6.5
13-4	12	2.17	179	92	7.2
13-5	7	2.17	132	85	9.0
Run 14 (Inlet CH_4 Concentration = 5 Per Cent; Temperature = 2000°C)					
14-1	10	2.17	95	68	6.0
14-2	13	2.16	110	85	9.6
14-3	12	2.16	133	78	9.8
14-4	15	2.17	105	77	12.6
14-5	12	2.17	142	78	10.0
14-6	8	2.17	117	73	10.8
Run 15 (Inlet CH_4 Concentration = 2.5 Per Cent; Temperature = 2000°C)					
15-1	10	2.20	124	73	6.5
15-2	20	2.17	110	78	6.2
15-3	18	2.18	110	68	6.4
15-4	19 **	2.13	141	73	6.5
15-5	17 **	2.17	110	72	7.0
15-6	13 **	2.21	124	78	6.0
Run 16 (Inlet CH_4 Concentration = 2.5 Per Cent; Temperature = 1900°C)					
16-1	6	2.16	105	68	5.5
16-2	16	2.09	87	78	4.0
16-3	12	2.16	117	73	6.5
16-4	10	2.19	124	78	5.5
16-5	10	2.18	134	78	6.3
16-6	8	2.17	134	57	4.5
Run 17 (Inlet C_3H_8 Concentration = 2.5 Per Cent; Temperature = 2000°C)					
17-1	6	2.19	105	73	5.3
17-2	13	2.17	105	73	5.2
17-3	10	2.20	110	68	5.8
17-4	17	2.19	124	73	6.4
17-5	13	2.19	110	85	7.0
17-6	8	2.17	165	73	5.5

TABLE II (continued)

Sample No.*	Thickness (mils)	Density (gms/cc)	Crystallite Dimensions (Å) L_a	Crystallite Dimensions (Å) L_c	004 Peak Intensity (Relative Units)
Run 18 (Inlet C_3H_8 Concentration = 5 Per Cent; Temperature = 2000°C)					
18-1	16	2.07	87	60	2.5
18-2	24	2.02	87	57	3.6
No coating, only soot formed or sections 3-6.					
Run 19 (Inlet C_3H_8 Concentration = 2.5 Per Cent; Temperature = 2000°C)					
19-1	16	2.05	91	68	3.6
19-2	21	2.12	95	72	4.5
19-3	14	2.15	117	85	6.8
19-4	16	2.16	105	84	7.5
No coating on sections 5 and 6.					
Run 20 (Inlet C_3H_8 Concentration = 1.2 Per Cent; Temperature = 2200°C)					
20-1	16	2.17	100	78	7.4
20-2	38	2.14	133	65	7.0
20-3	27	2.17	133	92	9.0
20-4	28	2.17	105	92	9.0
20-5	24	2.17	124	85	8.8
20-6	16	2.15	117	92	9.0
Run 22 (Inlet CH_4 Concentration = 5 Per Cent; Temperature = 2400°C)					
22-1	10	2.16	141	85	8.6
22-2	17	2.14	110	92	8.3
22-3	11	2.11	124	98	9.0
22-4	8	2.08	153	98	8.9
22-5	6	2.11	141	92	7.0
22-6	5	2.15	124	98	8.3
Run 23 (Inlet CH_4 Concentration = 2.5 Per cent; Temperature = 2400°C)					
23-1	8	2.14	141	78	7.4
23-2	16	2.14	165	68	5.1
23-3	12	2.16	141	85	8.7
23-4	12	2.18	117	78	8.8
23-5	17	2.20	133	85	10.6
23-6	12	2.17	141	78	8.0

* The 12-inch substrate was cut into 2-inch lengths numbered 1 to 6 from inlet end.
** Partial Delamination

The principal process variables that affect the deposition of pyrolytic graphite are the substrate temperature, the concentration or partial pressure of the carbonaceous source gas, and the gas dynamics over the substrate. The results of the basic process studies are discussed under several headings according to the characterization methods used. The general effects of the process parameters on the properties of the coatings can be seen from this discussion. Studies of some of the practical effects of process changes are discussed further in the next section on process improvement work.

1. Crystalline Parameters

The X-ray diffraction analysis of a pyrolytic graphite coating yields the inter-layer spacing dimension and the crystallite size, both in the stacking direction and in the layer plane direction. Without exception, the pyrolytic graphite deposits produced in these studies had an inter-layer d-spacing very close to 3.45 Å. This value is typical of that found for turbostratic structures in graphite. The fact that no inter-layer spacings less than 3.45 Å were measured indicates that three-dimensional ordering characteristic of the true graphite crystal is not present. This is consistent with the absence of three-dimensional diffraction peaks in the X-ray diffraction patterns. Other investigators have occasionally reported d-spacings as small as 3.40 Å indicative of partial graphitization or three-dimensional ordering. However, there is no evidence that the smaller d-spacing would produce superior properties in pyrolytic graphite; the turbostratic structure is a highly anisotropic structure in itself.

As determined by X-ray diffraction measurements, the average crystallite dimensions in the stacking direction and in the layer planes vary over a reasonable range with process conditions. The values for most sections of the substrate from each deposition run are listed in Table II. The L_c values range from about 60 to 90 Å. Based upon our present knowledge of the importance of this parameter, an average value of 75 Å would seem to represent adequately all the materials produced. The values of L_a range from about 90 to 150 Å. Here an average value of 120 Å would appear to define all of the materials adequately. For the later runs, the relative intensity of the 004 peak is listed for each sample. This value is thought to be related to the degree of crystallinity.

2. Density

The densities measured for the pyrolytic graphite coatings produced in this laboratory study range from 2.08 to 2.25 gm/cc. Increased temperature of deposition yields a higher density material on the average although some scatter exists. It is interesting to note, however, that while the theoretical density of true graphite is 2.26 gm/cc (d-spacing of 3.354 Å), the theoretical density for a turbostratic graphite-type structure with a layer spacing of 3.45 Å is only 2.19 gm/cc. Thus, all of the densities measured lie very close to this theoretical density; that is, the porosity of the pyrolytic graphite is near zero. This very low porosity undoubtedly is important in making pyrolytic graphite a very inert form of carbon in high-temperature environments.

3. Microstructure

When a polished cross-section of the pyrolytic graphite deposit is microscopically examined, a columnar or conical growth pattern is apparent. These growth "cones" are characteristic of pyrolytic graphite. No other single feature of this material is believed to be more important in determining the usefulness of a pyrolytic graphite deposit. The cones in the microstructure, as seen by normal metallographic procedures, are too large to be single crystallites. However, the conical microstructure does represent the interaction of the growth of pyrolytic graphite from various domains on the substrate or within the coating.

Examination of a large number of photomicrographs of the microstructure of pyrolytic graphite deposited under a variety of conditions indicates that there are several types of conical microstructures. In some samples, large cones which persist from the substrate through the coating to the surface comprise the major microstructure. In other coatings, smaller cones, some of which start above the substrate within the coating, are apparent. In still other coatings, the cone structure is very fine and appears to regenerate throughout the coating thickness. These various types of microstructure appear to be important because of the relation between the microstructure and the presence of small cracks or delaminations in the coating. When large primary cones are present in the microstructure, delamination cracks through individual grains are usually apparent. Often, these cracks join to produce longer,

more severe delamination cracks. In general, when a fine grain or regenerative cone structure is present, these delamination cracks are minimized and seldom are large areas of delamination apparent. Process improvement consists principally of developing practical means of producing a serviceable microstructure under the simplest process conditions. At the conclusion of these basic studies, it appeared that the fine-grained, regenerative microstructure would always be preferable to the large-cone, primary type of microstructure.

Actually, there are many variations of microstructure between the clean, large primary-cone structure and the fine regenerative structure. Indeed, the microstructure of a pyrolytic graphite deposit usually is some mixture of these types of microstructures, and it is not easy to define the precise conditions necessary to produce a given microstructure. Unfortunately, the deposition of pyrolytic graphite is complex, because of the effect of local gas dynamics and substrate geometry. Thenucleation and growth process is also sensitive to many small changes in operating conditions.

The balance between the rates of nucleation and deposition influences the size of the cones in pyrolytic graphite microstructure. Therefore, the concentration of the carbonaceous source gas, the temperature of the substrate, and the flow rate of the gas over the substrate are all variables of importance in their effect on microstructure. Figures 3, 4, and 5 show the effect on microstructure of changing the concentration of methane in the gas used t deposit pyrolytic graphite. Figure 3 shows a large primary cone structure obtained with a concentration of 14 per cent methane. The two horizoneal dark bands through the coating are delamination cracks which are extensive in this coating. In Figure 4, the microstructure produced with a 6 per cent methane concentration, is shown. Here the structure has clearly become finer, and no cracks are visible in the field of view. In Figure 5, the microstructure produced with a 2.5 per cent methane concentration is shown. Here the microstructure is quite fine and regenerative although a background of primary cone structure is still apparent. A few small interlaminar cracks are apparent in the larger cones. In each of these three deposition runs, the temperature and gas flow conditions were held constant. Since the concentration of the carbonaceous source gas has a direct relation to the deposition rate, its influence on the microstructure of the pyrolytic graphite deposits is to be expected.

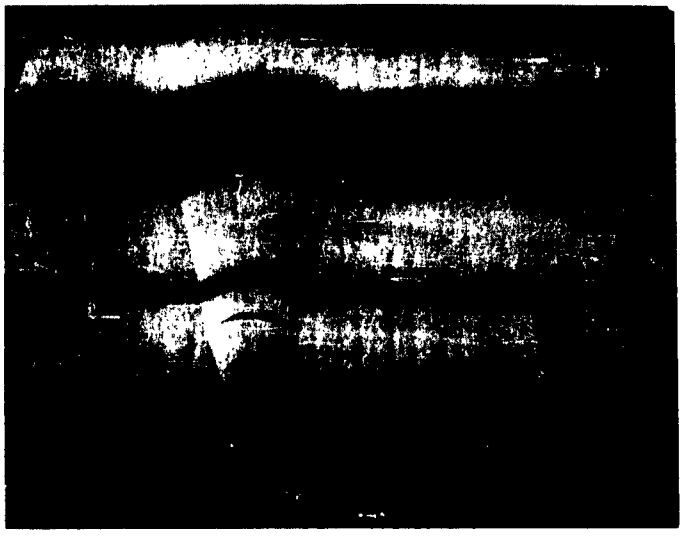

140-2

Figure 3. Pyrolytic Graphite Microstructure 14% CH_4, 2000° C, Specimen 7-2 (45X).

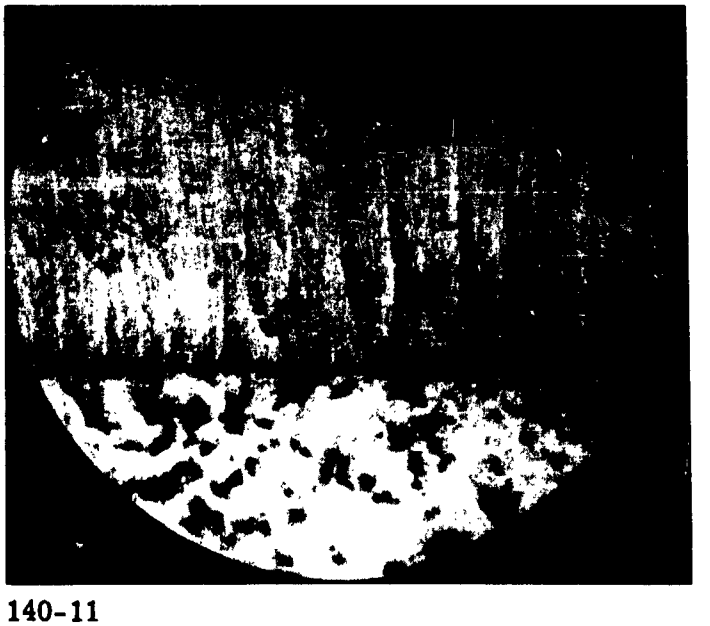

140-11

Figure 4. Pyrolytic Graphite Microstructure 6% CH_4, 2000° C, Specimen 8-4 (120X).

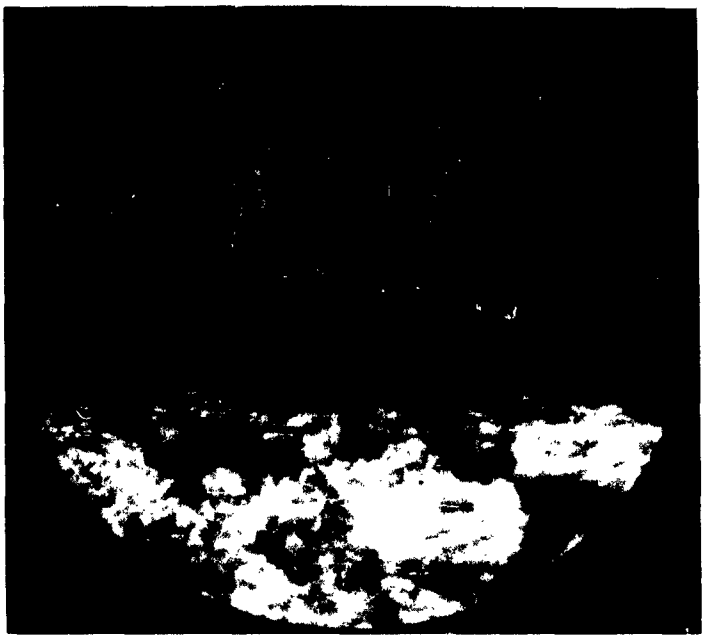

13-12

Figure 5. Pyrolytic Graphite Microstructure
2.5% CH_4, 2000°C, Specimen 12-4 (185X).

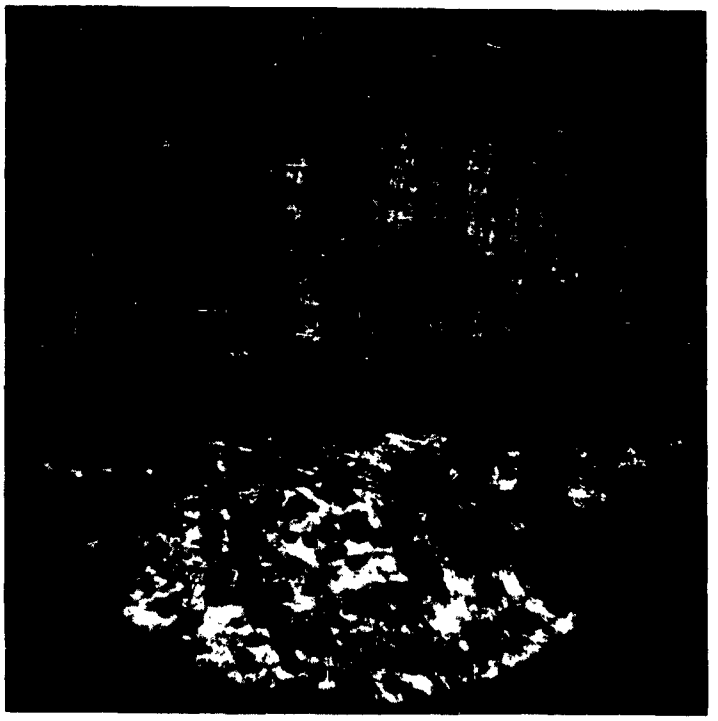

54-5

Figure 6. Pyrolytic Graphite Microstructure
6% CH_4, 2200°C, Specimen 9-2 (75X).

The temperature of the substrate upon which the pyrolytic graphite is deposited does not appear to have a dominant effect on the type of microstructure obtained in the temperature range from 1900°C to 2400°C. Figure 6 shows the microstructure of a deposit prepared at 2200°C. The other conditions for this deposition test were the same as those used for the deposit produced at 2000°C., shown in Figure 4. Although there is some qualitative difference in the microstructure, it is not clear that any significant difference exists. The difference in these two microstructures is typical of that found from one temperature to another in the range investigated during our basic process studies, namely, from 1900°C to 2400°C. At temperatures below 1900°C the effect of temperature is much greater as discussed later in the section on process improvement.

The effect of the flow rate of the gas mixture over the substrate can be seen by comparing the microstructure in Figure 7 with that in Figure 4. In this case, all the conditions are comparable except that the flow rate used to deposit the coating shown in Figure 7 was only one-half that of the flow rate used for the deposit shown in Figure 4. The difference in these microstructures indicates that a finer, more regenerative microstructure was formed at the low flow rate. The effect of the flow rate and the gas distribution in pyrolytic graphite deposition must not be minimized. The deposition rate, the coating uniformity, and the over-all quality of a pyrolytic graphite coating are greatly affected by the gas dynamics over the substrate.

4. Rate and Uniformity of Deposition

In the basic process studies, the deposition rates of pyrolytic graphite were not of primary concern. However, when fabrication of coated nozzle parts is required, a knowledge of the deposition rate is necessary so that proper coating thickness can be applied. Thus, correlation of the deposition rate with process conditions is helpful.

The deposition rates obtained in each of the isothermal deposition runs along with pertinent process conditions are shown in Table III. The same three major variables that affect the quality of the coating also appear to affect the rate of deposition. These variables are the substrate temperature, the carbonaceous source gas concentration, and the gas dynamics over the substrate. Above 1900°C the temperature of deposition appears to have relatively little effect upon the deposition rate. The decomposition of the carbonaceous

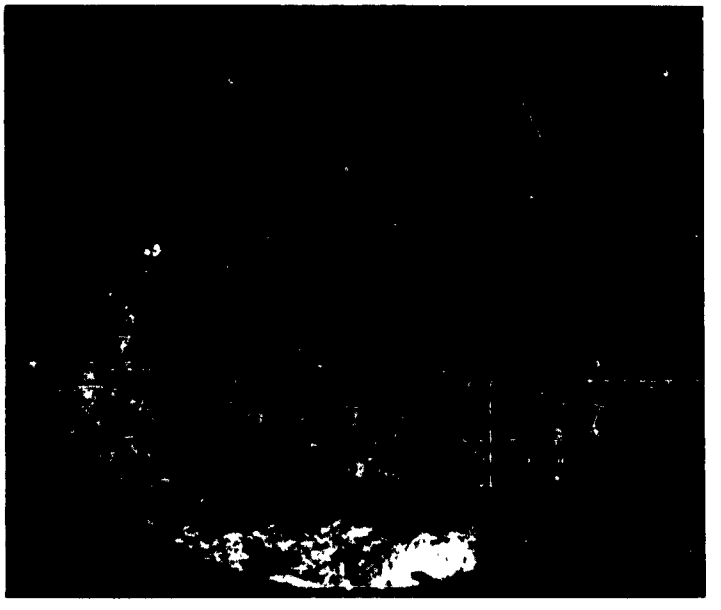

21-3

Figure 7. Pyrolytic Graphite Microstructure Low Gas Flow, Specimen 13-3 (185X).

TABLE III

Deposition Rates in Isothermal Deposition Runs

Run No.	Temperature (°C)	Source Gas Concentration (per cent)	Per Cent of Gas* Through Injector	Maximum Deposition Rate** (mil/hr)
7	2000	14 CH_4	60	19
8	2000	6 CH_4	60	12
9	2200	6 CH_4	60	15
10	2100	6 CH_4	60	16
12	2000	2.5 CH_4	60	5
13	2000	5 CH_4	80	5
14	2000	5 CH_4	90	8
15	2000	2.5 CH_4	90	5
16	1900	2.5 CH_4	90	5
17	2000	2.5 C_3H_8	90	8
18	2000	5 C_3H_8	90	12
19	2000	2.5 C_3H_8	90	10
20	2200	1.2 C_3H_8	90	9
22	2400	5 CH_4	90	6
23	2400	2.5 CH_4	90	4

* Total gas flow was 20 SCFH in all runs except Run 13 in which 10 SCFH was used.

** Deposition rate is calculated from mean thickness at the cross-section where maximum thickness occurred.

gas is rapid at the temperatures of deposition, and thus, the rate of deposit is controlled by the rate at which carbonaceous gas molecules reach the substrate surface. Consistent with this, the concentration of the source gas has a substantial effect on the deposition rate; the rate appears to be nearly proportional to the concentration of the source gas, other things being equal. Often overshadowing even the concentration effect, however, is the effect of the gas flow rate and flow pattern in the deposition zone. Local turbulence and impingement of the gas mixture on the substrate leads to high deposition rates since the carbonaceous source gas molecules are rapidly brought to the surface of the substrate.

In the basic process studies the geometry of the substrate was intentionally kept simple. Nevertheless, if the injector was not well centered in the substrate tube, uneven deposits were formed around the tube. With careful centering of the injector, uniform coatings at all radial positions could be achieved throughout most of the length of the substrate test section. The uniformity of the coating in the axial or flow direction can be varied by adjusting the concentration and flow rate of the gases, and by varying the flow through the injector and outside the injector in the annulus between the injector and the substrate tube. The variation in thickness of the coating along the axis of the substrate in each deposition test is given in Table II. In general, achievement of a uniform coating requires a moderately low coating deposition rate. In the course of this basic process study, when uniform coatings were achieved, the deposition rate was approximately 5 mils per hour. Although this is a reasonably slow deposition, no effort was made to increase this rate.

D. RESULTS FROM PROCESS IMPROVEMENT STUDIES

A continuing effort of moderate proportions was made during the second year to define certain relationships of interest in the deposition process. This effort was essentially a process improvement study. The deposition tests that were made were chosen for one of two reasons. Some of the tests were made in direct support of the nozzle preparation work. The remaining tests were made in an effort to define process conditions which might lead to substantial simplification of the deposition process, or to substantially different properties in the pyrolytic graphite.

All of the tests in the process improvement study were carried out using tubular substrates (one-inch inside diameter) in the same fashion as the basic process work. With this configuration the examination of the coating could be readily accomplished, and any changes in the coating, in either radial or axial directions, became apparent. The results of the process studies carried out after the first year's work are discussed under several headings below according to the principal effect being studied.

1. Effect of Gas Flow and Surface Finish

The thickness and uniformity of the pyrolytic graphite coatings are sensitive to the gas dynamics in the deposition zone. To prepare nozzle test pieces of the desired quality and configuration, the effects of gas dynamics and surface finish were studied. Twelve deposition runs were made in this series as shown in Table IV. All these runs were made with methane as the carbon source with a total gas flow rate (methane plus diluent) of 20 SCFH.

The rate of deposition of pyrolytic graphite is affected by the methane concentration. But of greater importance is the effect of gas distribution on uniformity of coating. In general, an expansion tip on the gas injector appears to improve gas distribution and the contol of coating uniformity. However, in Run 34 when all the process gas entered through the injector, a heavy deposit was formed over the first four inches of the substrate with a thinner, non-uniform deposit over the remainder of the substrate. In Run 33, a non-uniform deposit was formed by passing 40 per cent of the total gas through the annulus. The non-uniformity appeared as a slightly thicker coating at the outlet end of the substrate. In Run 32, a very uniform deposit was obtained by passing 10 per cent of the total gas flow outside the injector.

Control of the uniformity of the coating in the radial direction is also important. Careful centering of the injector in the substrate tube helps to produce good results. Provision was also made to rotate the substrate relative to the injector to allow additional control of the radial uniformity.

The surface finish of the substrate, in the range from 80 to 400 grit, does not appear to affect the coating greatly except that the finish of the coating reflects the substrate finish. The substrate surface roughness might be expected to affect the bond strength between the pyrolytic graphite coating and the substrate, but this effect was not studied.

TABLE IV

Effect of Gas Flow and Surface Finish

Run Number	Temperature (°C)	Substrate Surface Finish (grit)	Gas Injector Expansion Tip	Inert Diluent Outside Injector (per cent)	Inlet Methane Concentration (per cent)	Mean* Deposit Rate (mils/hr)
24	2000	320	Yes	10	2.5	2.5
25	2000	80	Yes	10	6	6.5
26	2000	80	Yes	10	5	6.5
27	2000	80	Yes	40	5	5.0
28	2000	80	No	40	5	5.5
29	2000	80	No	40	7	7.5
30	2000	320	Yes	10	5	5.5
31	2000	400	Yes	10	5	5.0
32	2000	320	Yes	10	5	5.0
33	2000	320	Yes	40	5	5.5
34	2000	400	Yes	0	5	15.0
35	1900	80	Yes	10	5	4.0

* At cross-section where maximum thickness occurs.

In line with the results of these deposition tests and the basic studies reported above, the standard grade pyrolytic graphite for nozzle testing was defined as that produced on a substrate with a normal machined finish at 2000°C from a mixture of methane and argon gas with 5 per cent methane by volume. Such deposits are uniformly of good quality and moderately fine-grained microstructure.

2. Effect of Deposition Temperature

Since optimization of the process conditions was assigned reduced priority after the first year of the program, emphasis was placed on those changes in process conditions which might produce substantial reductions in the cost or complexity of the production process, or which might produce pyrolytic graphite of markedly different physical or chemical properties. One method by which the deposition process could be substantially simplified would be the reduction of the deposition temperature. Power requirements, of course, would decrease and furnace requirements would be simpler. Residual stresses should be somewhat less and anisotropy should decrease. Although decreased anisotropy is not necessarily desirable in all respects, one advantage to be expected is greater transverse strength.

To evaluate the possibility of preparing pyrolytic graphite coatings at lower temperatures, a series of deposition runs was made with substrate temperatures in the range 1100-1700°C. The total gas flow for each run was 20 SCFH with 10 per cent of the flow being introduced outside of the cooled gas injector. The gas flowing outside the injector was argon only and was the quantity found to be optimum for deposition runs at 2000°C. No effort was made to determine whether or not the proper distribution of gas within and outside of the injector for low temperature deposition was the same as for 2000°C deposition.

The results of the low temperature deposition tests and the conditions used in each run are shown in Table V. It is apparent that the deposition rate is substantially reduced as the substrate temperature is reduced. The absolute values of the deposition rate apply only at the section of maximum coating thickness, and no particular attempt was made to obtain uniform coatings. The trend with reduced temperature is clear, however.

TABLE V.

Deposition Runs at Lower Substrate Temperatures

Run Number[a]	Temperature (°C)	Carbon Source Gas	Inlet Carbon Source Gas Concentration (per cent)	Mean Deposit Rate[b] (mils/hr)
36	1700	Methane	5.0	10.7
37	1500	Methane	5.0	4.5
38	1300	Methane	5.0	2.0
39	1100	Methane	5.0	No deposit
40	1300	Propane	2.5	3.0
41	1300	Propane	2.5	3.0

a. For all runs:
   1. 10 per cent of gas flow entered outside of injector.
   2. Substrate surface finish 80 grit.
   3. Total gas flow = 20 SCFH.

b. At cross-section where maximum coating thickness occurs.

At 1100°C no measurable coating was found after the two-hour deposition run. Propane was substituted for methane in Runs 40 and 41 to see if the less thermally stable propane would produce a more rapid coating at 1300°C. The observed deposition rate was proportional to the atomic concentration of carbon in the source gas and indicated no increased deposition rate from the use of propane.

The effect of reduced deposition temperature on the microstructure of the coatings can be seen in Figures 8 and 9. Lowering the substrate temperature encourages the formation of large, erratic cone structures. Such a coating is likely undesirable because of the surface roughness and the greater number of spearations within the cones. At 1300°C the coatings produced from either methane or propane show erratic cone growth. At 1500°C and 1700°C the coatings are much smoother and finer grained. At substrate temperatures up to about 1500°C the catalytic effects of the substrate surface presumably assume greater importance in determining the local deposition rates than at higher temperatures.

3. Effect of Substrate Pretreatment

The effect of surface condition of the substrate on the microstructure of the pyrolytic graphite coating was studied in several sets of deposition tests. In the first set of tests, the effect of the graphitic nature of the substrate and its purity were observed. Pyrolytic graphite was deposited on three different substrates at 1340°C. Deposition conditions are given in Table VI. Photomicrographs of the polished cross-section of each coating are shown in Figure 10. The substrate in Run 42 was grade AGOT (National Carbon Company) which is a high-purity graphite produced for nuclear applications. In Run 43, the substrate was the standard grade of graphite pipe used in most of the studies to date. The substrate for Run 44 was commercial grade carbon pipe and was chosen because of the markedly less graphitization of this material (as measured by X-ray diffraction patterns) compared to the normal graphite pipe.

Run 36 1700°C 150X

Run 37 1500°C 150X

Run 38 1300°C 150X

Figure 8. Microstructure of Coatings Produced from Methane at 1300° to 1700°C

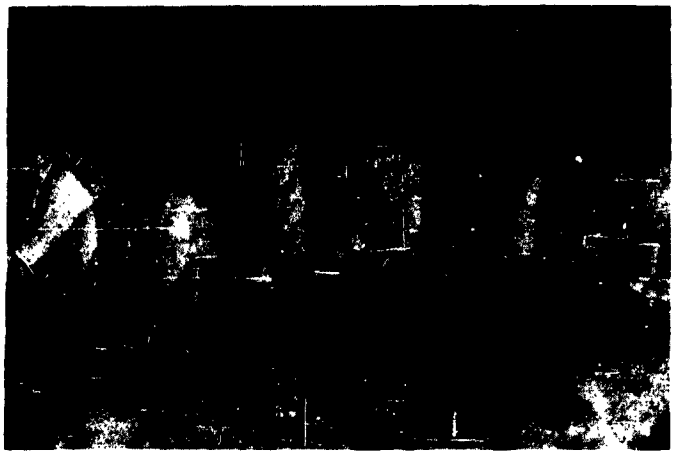

Run 40 1300°C 150X

Run 41 1300°C 150X

Figure 9. Microstructure of Coatings Produced from Propane at 1300 to 1700°C.

TABLE VI

Deposition Tests to Study Substrate Effects

Run Number[a]	Substrate Temperature (°C)	Substrate Material	Substrate Pretreatment	Carbon Source Gas	Source Gas Concentration (per cent)
42	1340	AGOT Graphite	None	Propane	2.5
43	1340	Graphite Pipe	None	Propane	2.5
44	1340	Carbon Pipe	None	Propane	2.5
45	2000	Graphite Pipe	Water-saturated Argon, 15 min at 2000°C	Methane	5.0
46	2000	Graphite Pipe	None	Methane	5.0
47	2000	Graphite Pipe	2500°C preheat for 2 hours	Methane	5.0
48	2000	Graphite Pipe	2500°C preheat for 4 hours	Methane	5.0
49	2000	Graphite Pipe	Honed precoat of Pyrolytic Graphite	Methane	5.0
50	2000	Graphite Pipe	Single impregnation of furane resin, carbonized, and honed	Methane	5.0
51	2000	Graphite Pipe	Double impregnation of furane resin, carbonized, and honed	Methane	5.0

a. Conditions common to each run
   1. Ten per cent of gas flow entered outside of injector.
   2. Total gas flow of 20 SCFH.
   3. Substrate surface finish, 80 grit.

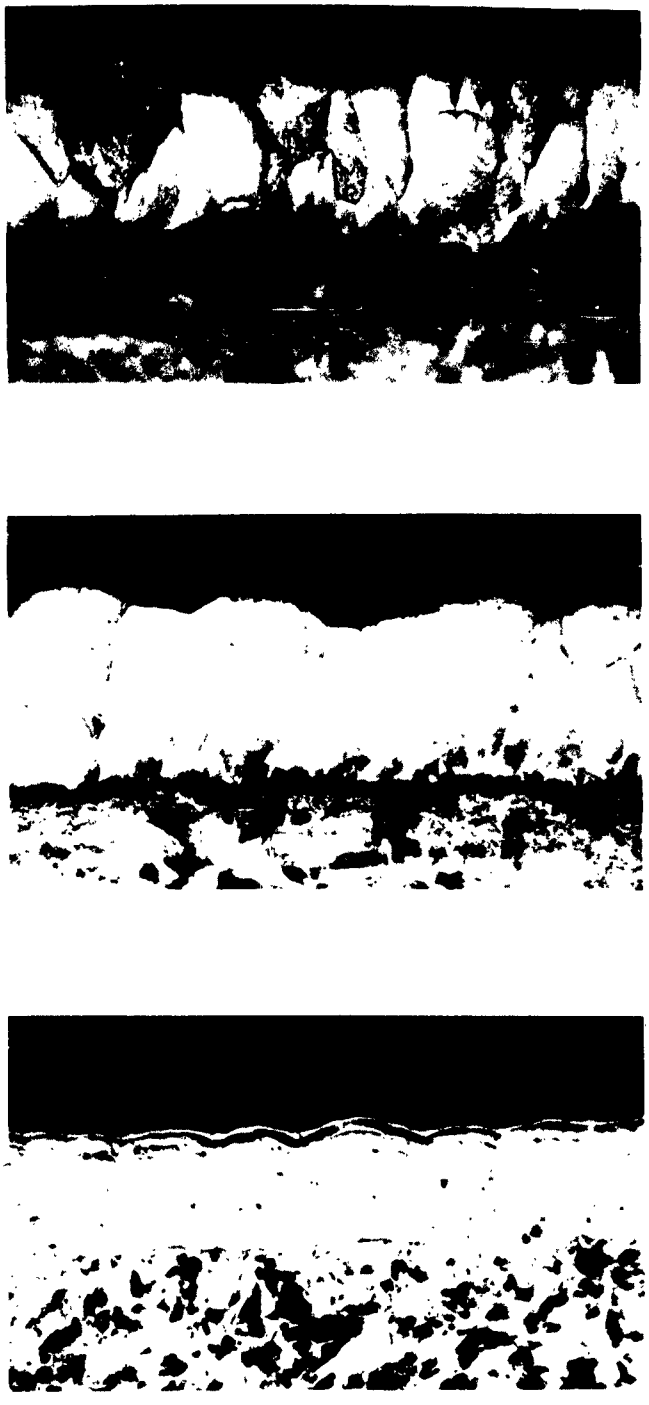

Figure 10. Microstructure of Deposits on Different Substrates at 1340°C.

The coating formed on each of these substrates was rather coarse, which is characteristic of the low-temperature (1340°C) deposit. However, the deposit on the less-graphitic substrate was somewhat finer-grained and was of a more uniform microstructure than that formed on the standard graphite substrate. The pyrolytic deposit on the AGOT graphite was coarser and rougher than that on the standard substrate, but this coarseness was probably caused, at least in part, by the rough surface of the AGOT material.

To obtain further data on the effect of surface condition on the coating microstructure, a second series of tests was carried out with a steam activation pretreatment of the substrate. For Run 45, a graphite substrate was exposed to argon saturated with water vapor at room temperature for 15 minutes immediately prior to deposition. The pretreatment and the deposition were both carried out at 2000°C. Run 46 was a control test in which all conditions were the same as Run 45 except that the steam pretreatment was eliminated. The deposit on the steam-pretreated substrate had an increased cone size, especially near the surface. Typical areas are shown in Figure 11. This increased cone size was probably caused by an increased activity of a number of reactive sites at which rapid nucleation and growth occurred. This is consistent with the activation process which would occur through steam treatment.

The results from both of these series of tests suggest that a uniform microstructure of reduced cone size requires a surface on the substrate which is moderately smooth and as uniformly inactive (chemically) as possible. Therefore, several other substrate pretreatment conditions, which might be expected to reduce the activity of the surface, were tested. Deposition of the pyrolytic graphite coatings was made of 2000°C in each case for convenience, although it is hoped that any technique found to improve the microstructure can be used at lower deposition temperatures. In Runs 47 and 48 little effect was noted from preheating the substrate for either two or four hours at 2500°C prior to the deposition test.

Figure 11. Effect of Steam Pretreatment on Microstructure of Pyrolytic Graphite

In Run 49 the substrate was precoated with pyrolytic graphite, then honed smooth, cleaned, and used for deposition tests. The line of demarcation between the precoat and the main pyrolytic graphite coating was very smooth and at some points difficult to identify. In other areas the cone structure changed across this boundary in such a way as to make it quite apparent. No particular evidence was found for poor bonding between the two layers of pyrolytic graphite, but the very smooth interface might lead to inadequate bond strength. One area of the coating produced over the pyrolytic graphite precoat is shown in Figure 12.

Another method of sealing the original graphite surface was tested in Runs 50 and 51. The substrates for these tests were impregnated with a furane resin which was then cured, carbonized to 1400°F, and honed smooth. The substrate for Run 50 had one impregnation, while the substrate for Run 51 had a double impregnation with the complete cure, carbonize, and hone cycle following each impregnation. This method of substrate pretreatment appeared to have a more obvious effect in reducing the number of large, wide angle cones found in the coating. These large cones are more susceptible to crack initiation in coatings of pyrolytic graphite. Unfortunately, in Run 50 in particular, coating delamination from the substrate occurred along a portion of the coating length. The very smooth substrate surface, as seen in Figure 13 may not promote good coating-to-substrate bonding. Nevertheless, the utility of resin impregnation pretreatment to reduce the incidence of large cones and improve the microstructure of pyrolytic coatings should be studied further, especially at lower deposition temperatures.

In review, only the pretreatments which seal and smooth the substrate surface, such as the pyrolytic graphite precoat or the resin impregnation, appear to offer much hope for a method to control the microstructure of pyrolytic graphite. The preliminary tests reported here suggest the need for further experimentation with the surface sealing pretreatments.

Run 49 150X

Figure 12. Pyrolytic Graphite Coating over Precoat of Pyrolytic Graphite

Run 50 150X

a. Single-Resin Impregnation

Run 51 150X

b. Double-Resin Impregnation

Figure 13. Coatings on Resin-Sealed Substrates

4. Ethylene and Acetylene Source Gases

In Runs 52 through 56 pyrolytic graphite coatings were prepared on normal graphite tube substrates at 2000°C and 1700°C using ethylene and acetylene as source gas. The conditions used in these deposition tests are listed in Table VII. A concentration of 2.5 volume per cent (equivalent in carbon atom per cent to 5 per cent methane) was found suitable to produce coatings very similar to those made from methane. On the basis of the limited number of tests carried out, no substantial advantage of either ethylene or acetylene over methane is apparent at the standard deposition temperature level. Structures of two sections selected from these deposition runs are shown in Figure 14.

5. Lower Temperature Deposition

The studies performed during the latter portion of the program were made primarily to determine the feasibility of preparing useful pyrolytic graphite at lower substrate temperatures than the 2000°C temperature normally used. If lower deposition temperatures were proved feasible the coating process could be carried out more easily. Reduced anisotropy and residual stresses should also be found in lower temperature deposits. However, the coarse grained irregular structure of the coatings normally formed at temperatures below about 1700°C is believed to be detrimental to good performance in a nozzle. Therefore, deposition tests were made with various source gases and with a resin-coat substrate pretreatment to see if improved microstructure could be obtained. The conditions used in these deposition tests are also listed in Table VII.

Even though no difference was discernible between coatings made with ethylene or acetylene and those made with methane at 1700° to 2000°C, it was felt that some difference might exist at lower deposition temperatures. Runs 57 through 60 were made at 1300 and 1500°C using ethylene and acetylene and normal graphite substrate tubes. The coatings prepared in these runs appeared to have a slightly more uniform microstructure than deposits produced earlier from methane. Still, the coatings formed at 1300°C appear too coarse to be serviceable. The deposits formed at 1500°C might prove to be useful. Figure 15 shows the structure of one of the coatings prepared at each temperature level.

29243

Run 54 1700°C Acetylene Source Gas (150X)

Run 55 2000°C Ethylene Source Gas (150X)

Figure 14. Pyrolytic Graphite Microstructure from Acetylene and Ethylene at High Deposition Temperatures

TABLE VII

Additional Deposition Process Studies

Run No.	Temperature (°C)	Carbon Source Gas	Inlet Carbon Source Gas Concentration (per cent)	Deposition Rate (mils/hr)	Substrate
52	2000	Acetylene	5	4.5	Graphite
53	2000	Acetylene	2.5	9.5	Graphite
52	1700	Acetylene	2.5	11.0	Graphite
55	2000	Ethylene	2.5	14.5	Graphite
56	1700	Ethylene	2.5	13.5	Graphite
57	1500	Ethylene	2.5	7.0	Graphite
58	1500	Acetylene	2.5	7.0	Graphite
59	1300	Acetylene	2.5	3.2	Graphite
60	1300	Ethylene	2.5	3.3	Graphite
61	1300	Methane	5.0	3.0	Furane-coated graphite
62	1500	Methane	5.0	6.1	Furane-coated graphite
63	1700	Methane	5.0	11.5	Furane-coated graphite
64	1500	Ethylene	2.5	6.7	Furane-coated graphite
65	1500	Acetylene	2.5	6.7	Furane-coated graphite

29244

Run 57 1500°C Ethylene Source Gas (150X)

Run 59 1300°C Acetylene Source Gas (150X)

Figure 15. Pyrolytic Graphite Microstructure from Acetylene and Ethylene at Low Deposition Temperatures.

To provide further information concerning coatings prepared at lower deposition temperature, the density of a number of samples was determined. The method used was the flotation procedure described earlier. Densities were measured for coatings prepared at temperatures ranging from 1300°C to 2000°C from several source gases (methane, ethylene, and acetylene) and on both plain substrates and furane resin-coated substrates. Figure 16 shows the range of densities found at the different temperature level.

Specimens were taken from sections of the standard 12-inch long substrate tube as close as two inches from the injector and as far downstream as eight inches from the injector. Much of the spread in density values shown in Figure 16 at the lower temperatures depended upon the axial distance from the injector. Examination of the data showed no strong effect on density of the source gas type or substrate condition. The most interesting conclusions from this study, however, are that coatings of relatively high density can be prepared over a wide range of temperature and that some control of the density appears possible. The dip in density at 1500-1600°C is similar to that observed by others, although the decrease in density found in our work is less than generally observed.

6. Lower Temperature Deposition on Pretreated Substrates

One promising substrate pretreatment consisted of coating the substrate with a furane resin. After the resin was cured it was carbonized to 1400°F and the surface honed smooth. In Runs 61 through 65 substrate tubes were used which had been pretreated in this fashion. Pyrolytic graphite was prepared from ethylene and acetylene at 1500°C and from methane at 1300, 1500, and 1700°C. In each case the coating microstructure was improved over that formed under similar conditions on an untreated substrate. In particular, the uniformity of the structure was improved. In Figure 17 the microstructures of the coatings prepared at 1500°C from methane and ethylene source gases are shown. It appears likely that pyrolytic graphite of this quality would be useful in rocket nozzle; however, the emphasis placed on motor tests of nozzles coated with the standard (2000°C) pyrolytic graphite and the scale-up of these nozzles precluded the testing of lower temperature coatings.

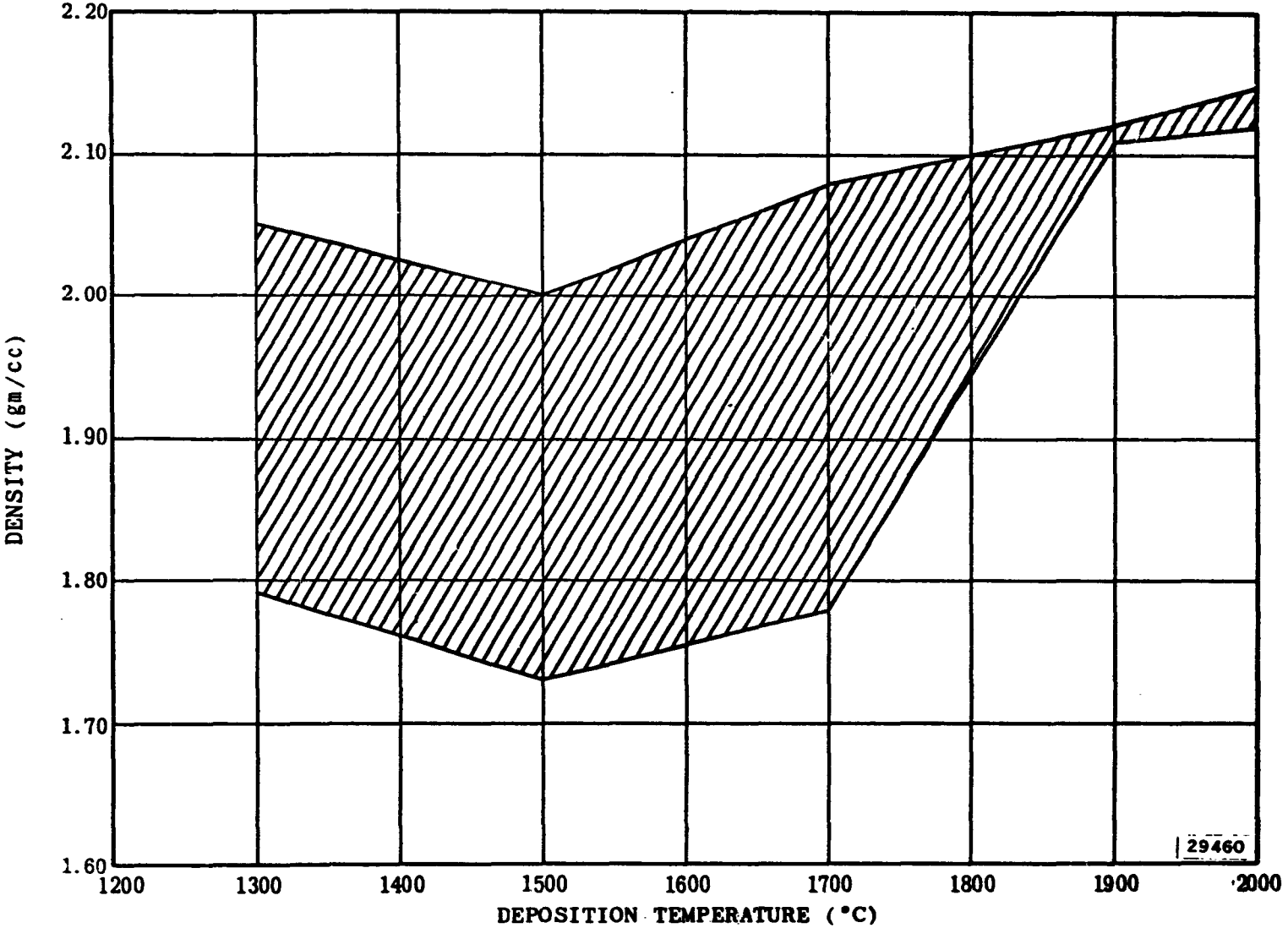

Figure 16. Density Range of Pyrolytic Graphite Coatings.

29245

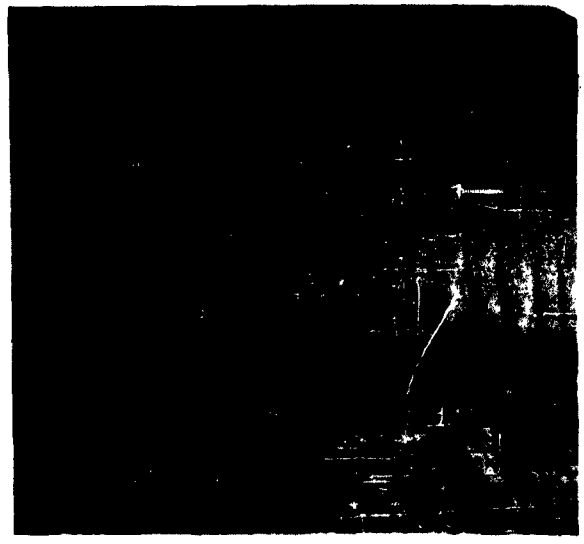

Run 62 1500°C Methane Source Gas (150X)

Run 64 1500°C Ethylene Source Gas (150X)

Figure 17. Pyrolytic Graphite Microstructure on Precoated Substrates at Low Deposition Temperatures.

V. MOTOR FIRING TESTS OF PYROLYTIC GRAPHITE NOZZLES

This phase of the program assumed major importance following the basic process study carried out during the first year. Accurate assessment of the inherent capabilities of pyrolytic graphite coatings in rocket motor nozzles required a carefully conceived and executed motor test program. The mode of failure of pyrolytic graphite had to be considered if meaningful data were to be obtained. The test techniques had to be selected with care so that the inherent "best" performance of pyrolytic graphite could be observed.

A. ANALYSIS OF FAILURE MECHANISMS

Prior to the start of nozzle testing on this program Atlantic Research had gained a considerable background and insight into the behavior of pyrolytic graphite through nozzle testing on a program for the Bureau of Naval Weapons. Using this work as a source of nozzle samples tested in rocket motor firings, one of the first tasks carried out on the current contract was to determine the mechanisms that cause failure of pyrolytic graphite coatings.

When pyrolytic graphite is used in rocket nozzles, failure may occur in several ways. Three distinct and separate mechanisms of material loss may be classified as follows:

1. Massive fracture and delamination
2. Spalling and minor delamination
3. Chemical and mechanical erosion

In massive fracture and delamination, the entire pyrolytic graphite coating may be lost, leaving the substrate material unprotected. This type of catastrophic failure is associated with poor bonding of the coating to the substrate. In turn, the poor bond is usually the result of improper mechanical design and mismatch of the properties of the pyrolytic graphite and its substrate. Figure 18 shows a nozzle after test in which the coating has come loose from the substrate. In this particular test the coating was retained throughout a successful test, but the mode of incipient failure is clear. This type of coating fracture, starting upstream of the insert throat, has been observed in larger scale nozzle tests. During motor firing, this type of failure is easily recognized by a sudden pressure loss followed by a steady decay in pressure as the substrate erodes.

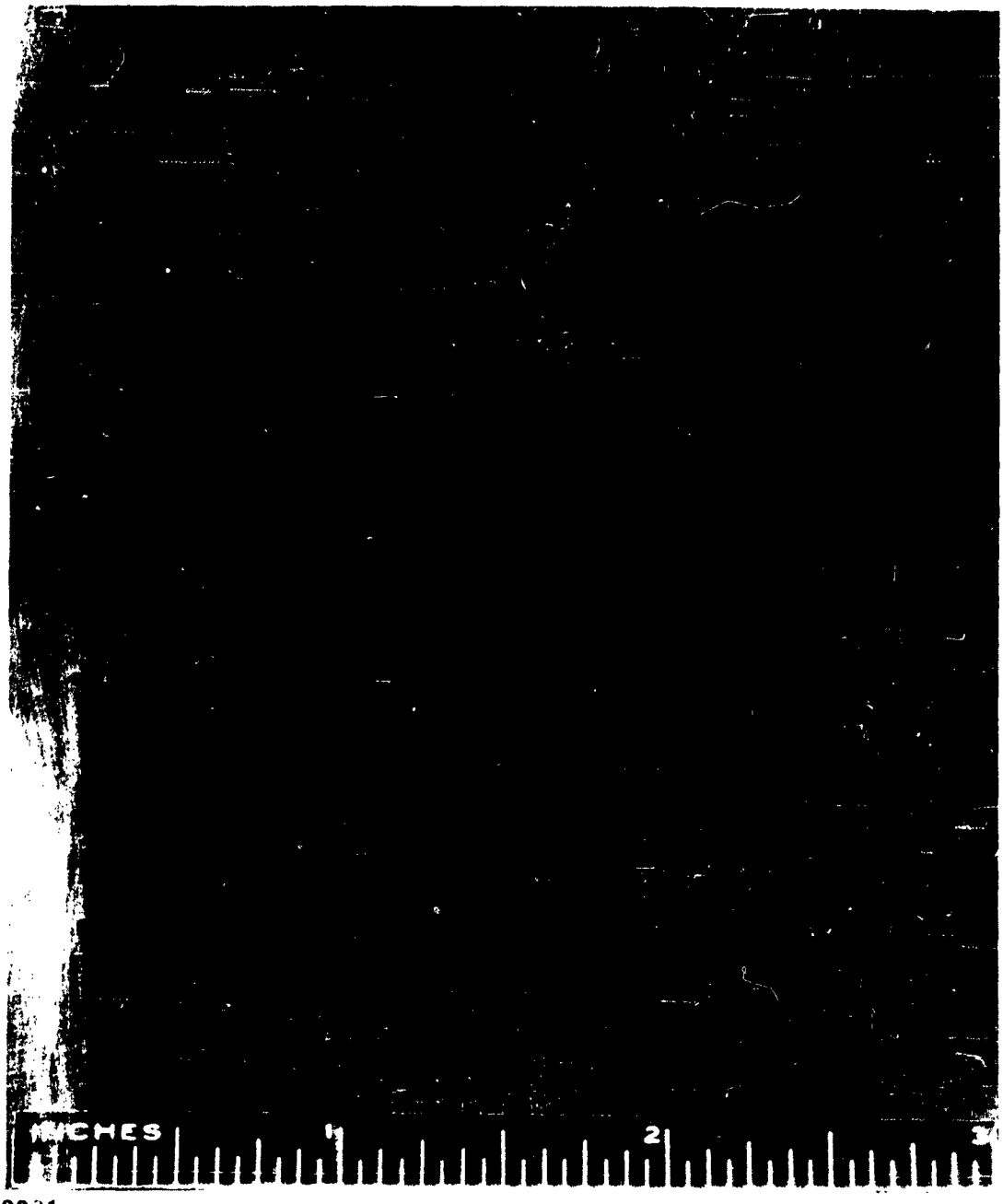

2381

Figure 18. Coating Delamination and Fracture

Some mismatch of physical properties is inevitable when pyrolytic graphite is mated to another material, although adequate design can minimize failures caused by these differences. One approach often suggested to avoid pre-stresses from the deposition provess is to remove the pyrolytic graphite coating from its deposition substrate and use it in free-standing form. This may be helpful in some cases, but proper design considerations are still required to prevent failure in service. Fracture and complete failure of a nozzle structure can still occur readily from stresses induced during service, especially from insufficient support and improper retention of the pyrolytic graphite shell. Stresses caused by thermal gradients and thermal expansion anisotropy are also significant.

The second type of failure noted with pyrolytic graphite nozzles consists of minor or local delamination cracking with the spalling of various size chips or slivers from the surface. The microscopic examination of the polished sections of a series of pyrolytic graphite coated nozzles tested in motor firings has shown the frequency with which this occurs. Whenever a large primary cone microstructure is found, the source of these delaminations is apparent. In Figure 19 three different photomicrographs of fired nozzles are shown to demonstrate this failure mechanism. Each of these views shows some portion of the coating which is near the point of being lost by spalling. When erosion occurs by this mechanism, the pressure trace from a motor firing usually shows a series of small but sharp decreases; in some cases, the erosion appears reasonably smooth but continuous and appreciable in extent. Although this mode of material loss does occur frequently and is often built into the pyrolytic graphite structure, it is not necessarily an inherent factor in the best grades of the material. It is considered as a separate and distinct mechanism because it can conceivably be avoided or at least greatly minimized.

The third mechanism in the failure of pyrolytic graphite is normal erosion by mechanical forces in the nozzle combined with chemical attack. This mechanism is meant to include only that erosion inherent and unavoidable in the material. In this sense it is entirely different from the first two mechanisms which are caused or accentuated by the design and preparation of the nozzle and may thus be eliminated under proper conditions. This third, "unavoidable" form of erosion represents the ultimate capability of the material and determines its maximum usefulness in nozzle service. If erosion is by this mechanism, the motor pressure trace should be smooth with the extent of regression being determined by the inherent material stability.

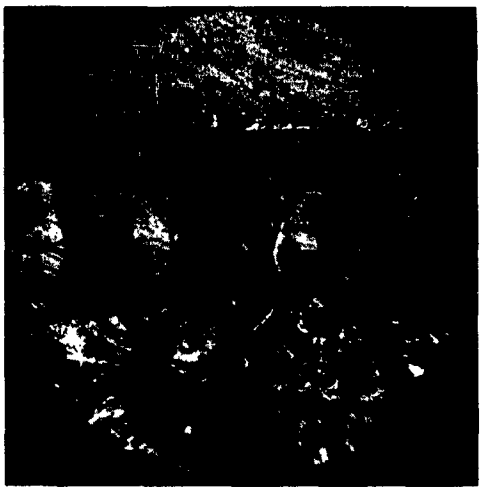

69-11

A. Large Cones and Cracks (40X)

69-9

B. Delamination (40X)

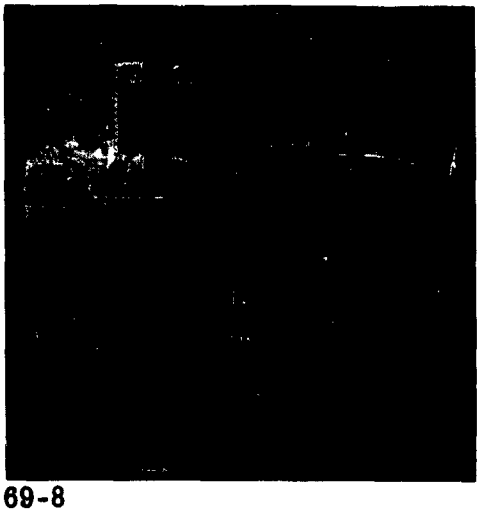

69-8

C. Cone Shifting (100X)

Figure 19. Delamination Cracks in Fired Nozzle Coatings.

In determining the usefulness of any material for nozzle service, the inherent stability of the material should be determined. This approach has generally been taken in trying to use very brittle materials, such as the refractory metal carbides, which must be reinforced and carefully retained to prevent thermal shock failure. Only after the problem of catastrophic failure and spalling have been solved can such materials be evaluated realistically. This is the approach which should be taken with a new material, such as pyrolytic graphite, which has rather unusual anisotropic physical properties.

B. MOTOR TEST METHOD

The most meaningful test of a pyrolytic graphite material for nozzle applications is an actual rocket motor firing. The correlation of property and characterization data with serviceability must be made on the basis of motor firing results.

In past work, Atlantic Research has motor tested a number of nozzles coated with pyrolytic graphite by several commercial producers*. In Arcite 373 propellant (5600°F, aluminized), these nozzles have given performance ranging from excellent to very poor. X-ray diffraction and density measurements have failed to show any significant differences that reflect in motor performance. Since the process conditions used in the deposition of the pyrolytic graphite were generally not available to us, no correlation could be made. In one instance, in which a series of pyrolytic graphite nozzle inserts were supplied with the deposition temperature specified (some at 1900°C, some at 2150°C), the better and poorer performance was evenly divided between the two temperature levels. This indicated that deposition temperature alone was not a controlling factor in serviceability for these particular nozzle inserts. It is clear that the best way to evaluate pyrolytic graphite is to integrate the deposition work and the motor testing. Only if the deposition conditions and techniques, together with the motor testing techniques and results are understood, can an improvement in the utility of pyrolytic graphite be made.

---

* These commercial producers include Raytheon, High Temperature Materials, American Metal Products, and General Electric.

In selecting a test nozzle configuration, three requirements were held to be of prime importance. First, the test must expose the nozzle insert to a thermal, chemical, and mechanical environment typical of solid-propellant rocket motor service. This requirement was easily met by choosing the test method developed on a program for nozzle insert evaluation for the Bureau of Naval Weapons. By using a nozzle insert of modest volume and by insulating this insert from the heat sink of the structural parts, a meaningful sub-scale test has been achieved. Since this test method has proved itself in our evaluation work, it was an obvious choice to motor-test pyrolytic graphite nozzles.

The other two requirements to be satisfied in motor-testing pyrolytic graphite deal with the preparation of the inserts themselves. Consistent with the discussion of the failure mechanism above, every effort should be made to determine at the outset the inherent serviceability of the material. In other words, spalling and delamination should be eliminated by any practical means so that the inherent erosion rate through chemical and mechanical attack can be measured. After this basic measurement is made, if the material still looks useful, the problem of designing and producing practical nozzle hardware can be undertaken. The final requirement is that pyrolytic graphite comparable to that actually under test in the motor should always be available for examination and characterization. Some of the characterization methods are destructive of the sample and cannot be applied to the nozzle before testing. In the past, no way has been available to examine the structure of a pyrolytic graphite in or near the critical throat region prior to testing.

A nozzle assembly which satisfies all three of the above requirements was devised for the initial motor tests as shown in Figure 20. The segmented nozzle insert consists of three separate pieces. For tests with Arcite 373 propellant (5600°F), the inlet and outlet sections can be made of molded commercial graphites since these will be eroded only moderately. The throat section consists of a pyrolytic graphite coated cylindrical washer, which can be cut from a coated substrate tube of proper inside diameter. By this technique, the edge of the pyrolytic graphite coating to be tested can be polished and examined microscopically both before and after motor firing. Furthermore, the coating immediately adjacent to the section tested in the motor is available for further testing, such as X-ray diffraction analysis. The use of a small

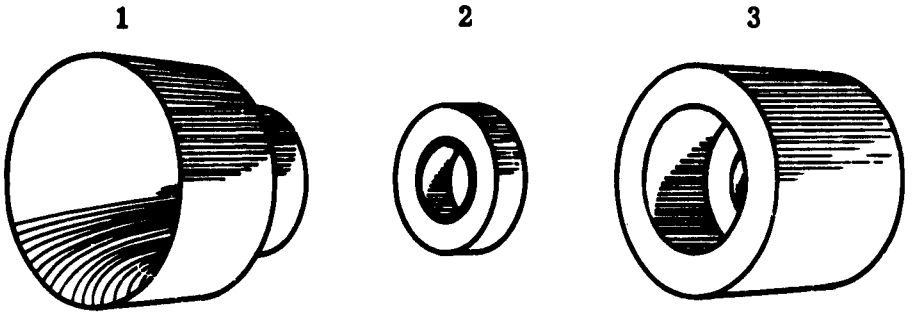

Exploded view of segmented nozzle insert
Part 1 - ZT Graphite
Part 2 - Pyrolytic Graphite Test Piece
Part 3 - ATJ Graphite

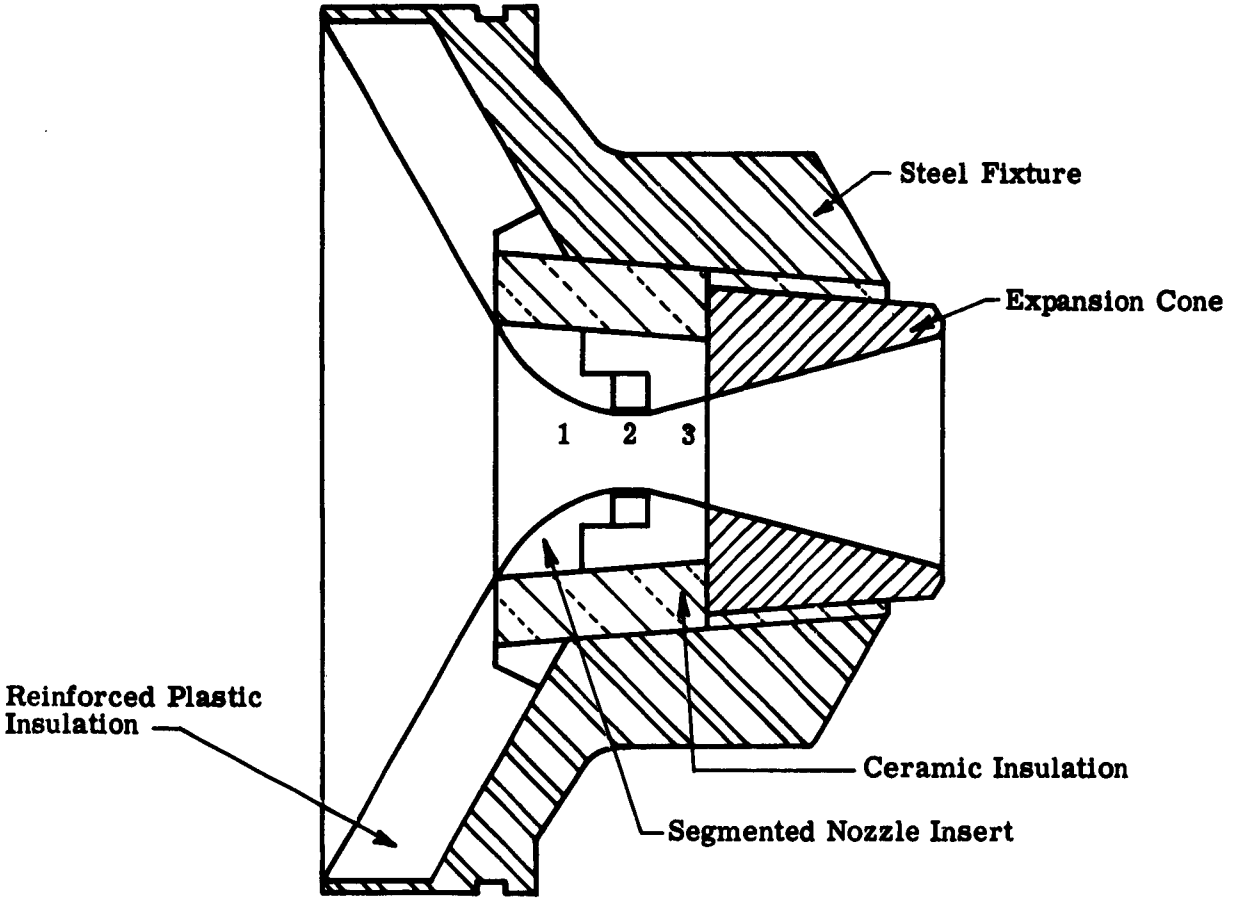

Figure 20. Nozzle Assembly with Segmented Nozzle Insert for Motor Tests with 5600°F Propellant

area of pyrolytic graphite on a cylindrical substrate at the throat (only) of the nozzle reduces to a low level the chance of coating loss or serious delamination. The selection of this segmented nozzle insert design satisfies fully the latter two requirements specified above.

The outer envelope of this nozzle insert conforms to the standard drawing used to fabricate test inserts for our general nozzle evaluation program. Thus, the pyrolytic graphite nozzle could be installed directly into the motor hardware that is standard at Atlantic Research. The use of this established test procedure in which the nozzle heat sink effect is minimized by the use of an insulating material for nozzle insert support assured that a realistically severe nozzle test would be made; this satisfies the remaining requirement set forth above.

The use of a segmented nozzle design provided several advantages. Nozzle insert preparation was kept simple and reliable, and microscopic examination of coating quality was possible at a point close to the nozzle throat. During the analysis of the shear stresses in coated sections which is described later in this report, it became apparent that a segmented design with a short coated length was especially useful in reducing the edge stresses. However, when propellants with flame temperatures of 6000°F or higher were used the pyrolytic graphite coating was extended a reasonable distance beyond the throat in each direction since no other graphitic material was sufficiently erosion resistant to serve near the throat. In our program this was accomplished by lengthening the coated throat section to 3/4 inch and contouring it to the standard nozzle shape. A cross-section of the nozzle insert used for motor tests with 6000°F and 6500°F propellants is shown in Figure 21. A photograph of the three pieces which form a segmented nozzle insert is shown in Figure 22 prior to assembly for motor test.

C. RESULTS FROM MOTOR TESTS

The primary data obtained from motor tests were the nozzle erosion rate and the associated operating parameters of the rocket motor. The majority of the tests were made with the standard (2000°C) pyrolytic graphite coating since the principal goal was the definition of the inherent capability of such a standard material under different motor operating conditions. In one firing,

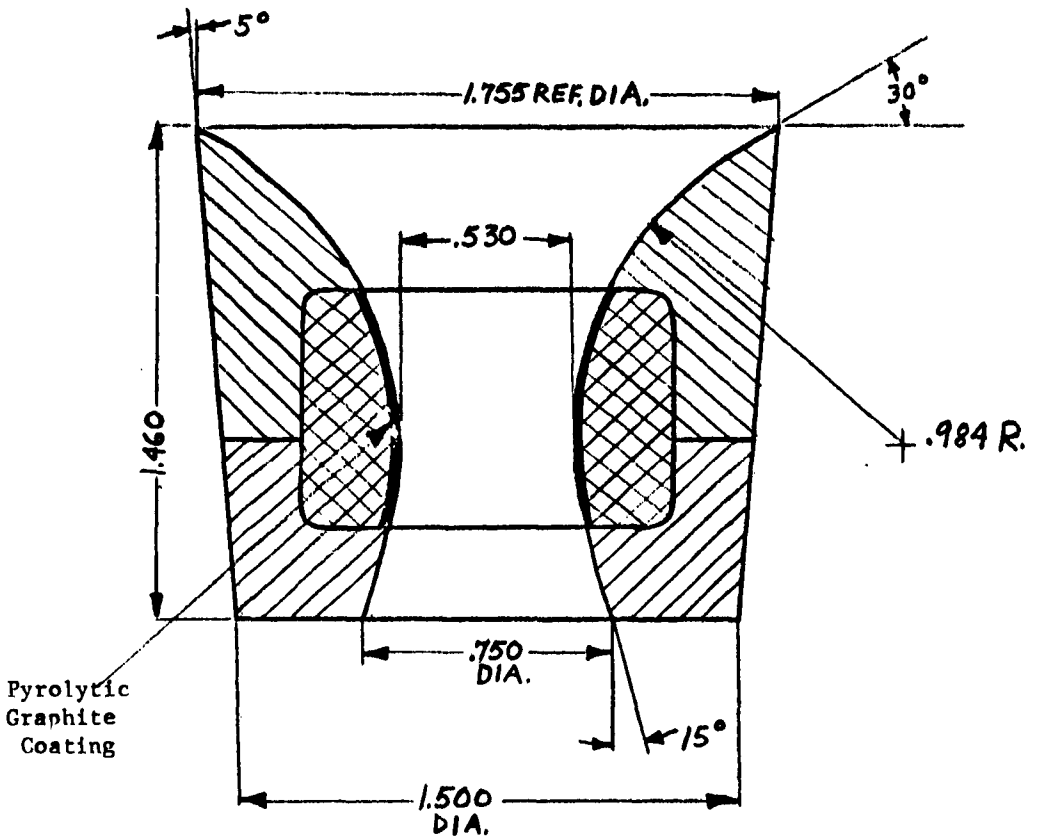

Figure 21. Detail of Segmented Nozzle Insert

Figure 22. Segmented Test Nozzle Before Assembly

PYM-3, a coating with a coarse microstructure was tested to find the effect of microstructure but this work was set aside in favor of the principal goal. In another test, PYB-6, a lower temperature coating (1700°C) was evaluated but this area of study was not pursued further.

Motor tests were made with aluminized solid propellants having theoretical flame temperatures of about 5600°F, 6000°F, and 6500°F. All but the last two firings were made with nozzles of nominal 0.530 inch throat diameter. The throat diameter was adjusted (about ± 40 mil) and the motor diameter was changed as needed to provide the range of operating pressure desired. The last two firings utilized nozzles of nominal 1-inch throat diameter to demonstrate the scale-up potential of pyrolytic graphite nozzles. The data from each firing are shown in Table VIII and discussed for each propellant system below.

1. Firings with 5600°F Propellant

The first propellant used in the nozzle test program was an aluminized Arcite formulation with a flame temperature of about 5600°F. This propellant, which is typical of many propellants currently in use in state of the art designs, has an oxidation ratio of 1.00 (defined as only sufficient oxygen content to convert Al to Al_2O_3 and C to CO).

Three motor tests of pyrolytic graphite were made with this propellant. The erosion rate of the standard 2000°C pyrolytic graphite was only about 0.1 mil/sec for a motor pressure of 1000 psi. These data from these tests are shown on Figure 23 which shows all the erosion rate data. The pyrolytic graphite specimens tested in firings PYM-1 and PYM-2 were both cut from a single coated tube. The section used in PYM-1 was as-deposited; the section used in PYM-2 had an overly thick coating and contained a delamination in the upper part of the coating. This coating was ground off to remove the delamination and reach the desired throat diameter. The firing results indicated no problem with this machining operation.

Prior to each of these motor tests, the coated nozzle section was polished lightly to allow an examination of the microstructure. Photomicrographs in Figure 24 show the microstructure before and after firing PYM-1. In both of the firings the molded ZT graphite used as the entrance section eroded sufficiently

TABLE VIII

Motor Test Data for Pyrolytic Graphite Nozzles

Firing Number	Pyrolytic Graphite Deposition Temperature (°C)	Motor Operating Conditions: Average Pressure (psi)	Motor Operating Conditions: Duration (sec)	Nozzle Erosion Rate (mil/sec)	Remarks
a) Tests with 5600°F, 1.00 Oxidation Ratio, Propellant					
PYM-1	2000	950	40	0.06	
PYM-2	2000	1150	29	0.15	
PYM-3	2000	917	62	0.16	Coarse-grained microstructure deposit
b) Tests with 6500°F, 1.08 Oxidation Ratio, Propellant					
PYB-1	2000	1150	9	--	Coating failed after 9 seconds
PYB-2	2000	830	21	0.48	
PYB-3	2000	350	36	0.00	
PYB-4	2000	468	66	0.52-0.66	Full nozzle coated: Lower erosion based on coating thickness
PYB-5	2000	650-750 (est.)	46 (est.)	0.36	Full nozzle coated: Erosion rate at minimum point because of local gouge
PYB-6	1700	322	68	--	Low temperature coating lost: Appears unserviceable in 6500°F propellant
PYB-7	2000	367	45	0.12	
PYB-8	2000	418	35	0.13	
PYB-9	2000	686	24	0.11	
PYB-10	2000	725	31	0.37	Coating 42 mils thick: Temperature instrumentation
PYB-11	2000	825	31	0.34	Coating 25 mils thick: Temperature instrumentation
PYE-1	2000	748	52	0.27	
c) Tests with 6000°F, 1.20 Oxidation Ratio Propellant					
PYC-1	2000	795	32	0.00	Leak at inlet at 32 seconds
PYC-2	2000	766	45	0.07	
PYC-3	2000	710	47	0.11	Coating 50 mils thick, temperature instrumentation
PYC-4	2000	735	44	0.09	Coating 27 mils thick, temperature instrumentation
PYC-5A	2000	840	61	0.27	Nozzle used was recovered from aborted firing PYC-5
PYC-6	2000	948	59	0.21	
PYC-7	2000	1167	30	0.54	One inch diameter nozzle
PYC-8	2000	829	56	0.42	One inch diameter nozzle
d) Tests with 6000°F, 1.00 Oxidation Ratio Propellant					
PYD-1	2000	642	59	0.00	
PYD-2	1700	604	43	0.11	Lower temperature coating appeared serviceable in this propellant
PYD-3	1700	619	52	0.09	Lower temperature coating appeared serviceable in this propellant

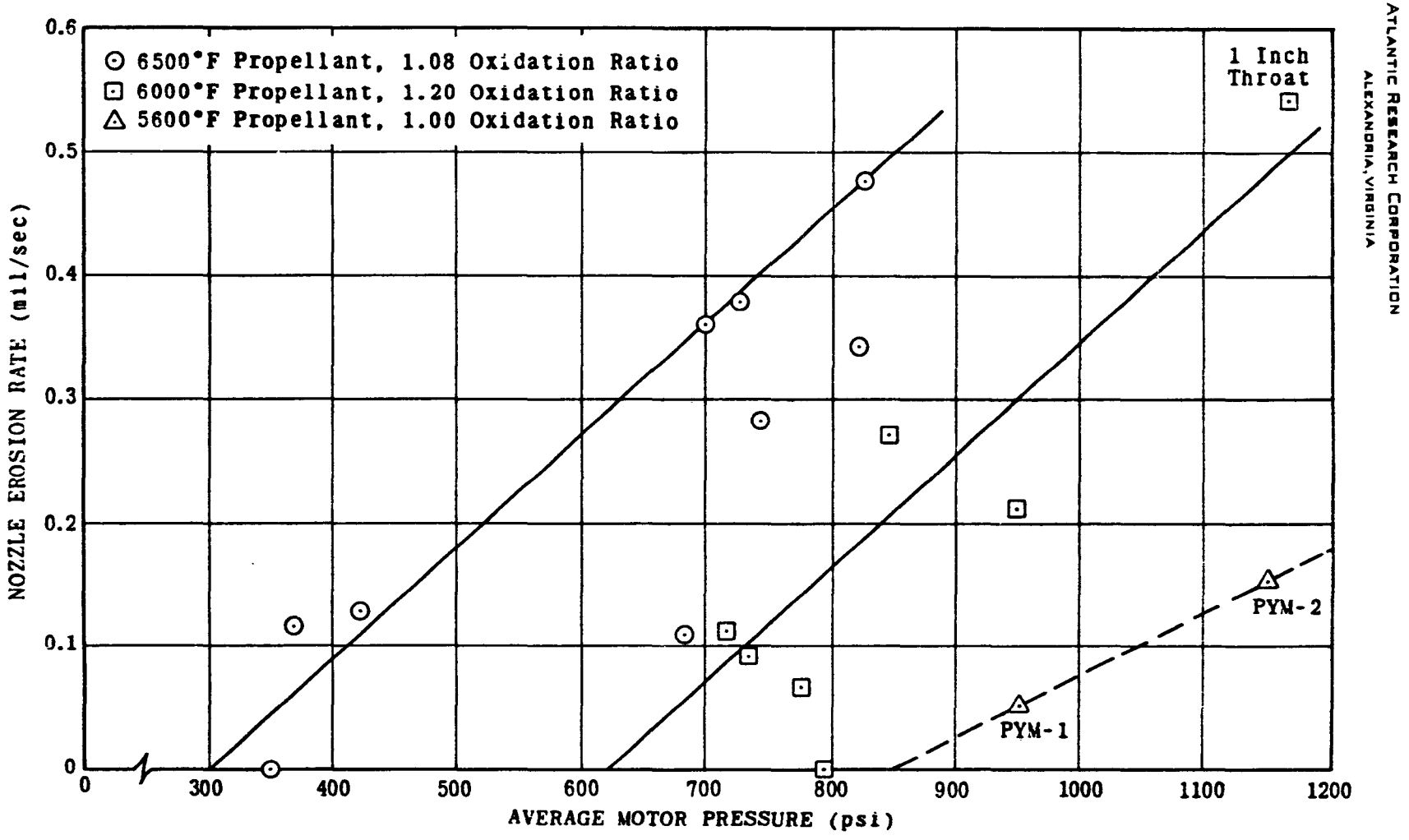

Figure 23. Effect of Motor Pressure on Pyrolytic Graphite Erosion Rate.

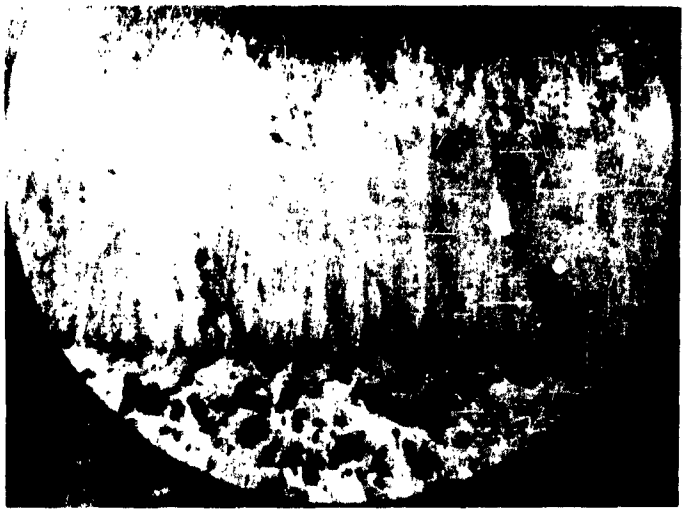

73-1

A. Before Motor Testing

74-11

B. After Motor Firing

Figure 24. Microstructure of Nozzle Test Specimen PYM-1

to expose the edge of the pyrolytic graphite in some areas at the upstream joint. This attack, which also occurred on the ATJ graphite used downstream of the nozzle throat, can be seen in Figure 25 which shows two views of the complete segmented nozzle insert from firing PYM-1 after test. Sufficient gas leakage occurred at the upstream joint in the nozzle to allow attack of the substrate behind the pyrolytic graphite, as can be seen by the large void in the after-firing photomicrograph (Figure 24). In spite of these factors, the coating performed in an outstanding fashion.

For the third motor test with this propellant, a coating of coarse microstructure was intentionally prepared. In firing PYM-3 this coating showed an erosion rate of 0.16 mil/sec at 917 psi, only slightly higher than the standard grade coating. Thus, these three test firings indicated that both the standard fine-grained coating and a coarse-grained coating can perform well in this 5600°F propellant if the coating is free of major cracks and delaminations. The equation of the line shown in Figure 23 is erosion rate, mil/sec = 5×10^{-4} (P_c-850) for P_c in psi.

It was apparent that a critical evaluation of the capabilities of pyrolytic graphite required motor tests with a hotter propellant. Since this evaluation of the serviceability of pyrolytic graphite over a range of severe motor conditions was the major goal of this work, the motor firing program was immediately shifted to tests with hotter propellants.

2. Firings with 6500°F Propellant

The segmented test nozzle used in the 5600°F propellant firings was modified for use with the 6500°F Arcocel propellant by lengthening the pyrolytic graphite coated section to prevent excessive erosion of the uncoated parts of the nozzle. No molded graphite is available which does not erode at a rather high rate when placed near the nozzle throat. Indeed, in early tests with the 6500°F propellant it was feared that coating failures might be initiated by excessive erosion of the molded graphite entrance section. Continued testing demonstrated that although substantial erosion always occurred in the molded graphite in the entrance area, the pyrolytic graphite coating was still able to perform its function as a low-erosion throat section.

Figure 25. Segmented Nozzle After Firing PYM-1
A. Entrance End B. Exhaust End

2859

A total of twelve motor firings were made with the 6500°F propellants which had an oxidation ratio of 1.08. In eleven of these tests, the standard 2000°C pyrolytic graphite coating was evaluated at different motor operating pressures. One test was made of a coating prepared at 1700°C; since this lower temperature coating was not serviceable with the 6500°F propellant, further testing of lower temperature deposits was deferred to permit the basic testing of the standard grade deposit.

The data from each of the motor tests with the 6500°F propellant are listed in Table VIII. The erosion rate measured in nine of the tests of the standard grade coating was considered reliable enough to define the effect of motor operating pressure as shown in Figure 23. This plot shows two facts of great interest concerning the capabilities of pyrolytic graphite. First, it can be seen that a good grade of pyrolytic graphite can give excellent service in rocket nozzles even at high pressure and high propellant flame temperature. An erosion rate of 0.5 mil/sec represents excellent performance, a level which very few materials can reach under such severe operating conditions. Second, the important role of motor operating pressure in causing nozzle erosion is clearly demonstrated. Indeed, the good performance noted at motor pressure near 1000 psi becomes essentially perfect at motor pressures of the order of 300 psi. The equation for the erosion rate line shown in Figure 23 is

$$\text{Erosion Rate, mil/sec} = 9 \times 10^{-4} \ (P_c - 300)$$

for P_c in psi.

One firing, PYE-1, was made with a different propellant formulation of 6500°F flame temperature. Although the ingredients used in this propellant were different, both the flame temperature and the oxidation ratio were the same. The lack of any significant change in erosion rate substantiates the postulate that the propellant flame temperature and oxidation ratio are the significant characteristics which determine the severity of a propellant environment towards pyrolytic graphite.

In three tests performed in the series with the 6500°F propellant, partial or complete nozzle failures occurred which should be commented upon. In firing PYB-1 the pyrolytic graphite coating was lost in about nine seconds. Prior to the loss of the coating the motor burned at an abnormally high pressure level; this excessive pressure undoubtedly contributed to the coating failure. A rather poor joint upstream of the contoured nozzle test piece may

also have contributed to this failure. This initial test with this propellant was the only coating failure experienced with the segmented nozzle design.

Two tests, PYB-4 and PYB-5, were made with fully coated, one-piece nozzles. These one-piece nozzles were prepared early in the firing program as a hedge against the problem of failure in the molded graphite entrance section of the segmented nozzles. In test PYB-4, the pyrolytic graphite coating was eroded through in the 66.2 second firing duration. The average erosion rate of 0.65 mil/sec was naturally greater than that to be expected from the coating alone because of the rapid erosion of the unprotected substrate toward the end of firing. However, even the erosion rate of 0.52 mil/sec based on removing just the coating appears higher than anticipated for the moderate average pressure in the motor chamber during this test (468 psi). Thus, the quality of this coating remains suspect with the probability that some spalling, rather than uniform erosion, of the coating occurred during firing. The erosion rate for this test thus lies above the line in Figure 23 which represents coatings of good performance. During firing PYB-5, the backing material failed locally and produced a gouge in the nozzle which introduced some uncertainty in the calculated erosion rate. Assuming that the minor diameter of the fired nozzle (approximately 90° from the gouged area) represents the basic erosion pattern for this test, an erosion rate of 0.36 mil/sec was calculated. The average chamber pressure during the test also is somewhat uncertain because of an instrumentation difficulty. The average was calculated from ballistic considerations with the uncertainty being at most ± 50 psi. This point fits with the remaining data and is in close agreement with firing PYB-10.

3. Firings with 6000°F Propellant

Motor tests of pyrolytic graphite nozzles were made with two different 6000°F propellants. One formulation had an oxidation ratio of 1.00 while the other had an oxidation ratio of 1.20. Three firings were made with the low oxidation ratio formulation. In PYD-1 a standard 2000°C coating showed no erosion at 642 psi average pressure. In motor tests PYD-2 and PYD-3 pyrolytic graphite coatings prepared at a substrate temperature of 1700°C on ATJ and AUC grade graphites, respectively, were tested at about 600 psi motor pressure. The low erosion rates observed for these lower temperature coatings (about 0.1 mil/sec)

indicated that in this propellant environment such coatings could perform well; this contrasts with the poor serviceability of the 1700°C coating noted in firing PYB-6 with the 6500°F propellant.

The remainder of the motor tests with 6000°F propellant were made with the high oxidation ratio formulation. It appears likely that practical propellants of high performance will be oxidizer-rich so that this more severe environment was a realistic choice for the critical evaluation of the capabilities of pyrolytic graphite. In addition to the three firings mentioned above with the low oxidation ratio formulation, six motor firings were made with nominal one-half inch nozzles with the high oxidation-ratio formulation. The data from these motor tests are included in Table VIII. The two firings using one-inch nozzles were also made with this high oxidation-ratio, 6000°F propellant. Data from these tests are included in Table VIII but the discussion of the results of the larger nozzle firings is contained in a later section of this report.

It can be seen from the results of the nozzle tests that pyrolytic graphite coatings show excellent serviceability under severe motor operating conditions with the 6000°F propellant. The erosion rate correlation with motor pressure shown in Figure 23 for this propellant is defined by the following equation:

$$\text{Erosion Rate, mil/sec} = 9 \times 10^{-4} \ (P_c - 620)$$

The motor pressure, P_c, is expressed in psi. A material which shows negligible erosion in firings with this propellant up to 600 psi motor pressure is an outstanding candidate for uncooled nozzle service. No monolithic commercial graphite, even those of very high density, has been found which even approaches this level of performance.

4. Effect of Coating Thickness on Erosion Rate

Throughout this program the selection of pyrolytic graphite coating thickness was made on the premise that the lowest thickness which could provide full-duration protection of the substrate would be the best choice. Unnecessarily thick coatings increase the opportunity for delamination to occur and permit higher surface temperature during service. However, since some additional coating thickness in excess of the anticipated total radial erosion must be used to provide a reasonable margin of safety, a series of four nozzle tests was made to investigate the effect of coating thickness on erosion rate. Two tests (PYC-3 and PYC-4) were made with the 6000°F, high oxidation ratio propellant

and two tests (PYB-10 and PYB-11) were made with the 6500°F propellant. The erosion data reported in Table VIII indicate no significant difference in the erosion rate between the nominal 25 mil coatings (the standard value used for the majority of the tests) and the 40-50 mil coatings. Slightly higher erosion rates were found for the two thicker coatings and this is certainly the direction of any anticipated effect since the surface temperature would be higher for the thicker coatings.

5. Temperature Measurements from Nozzle Tests

Temperature-time histories were measured at the back of the coated throat section of the segmented nozzles during the four motor firings made to study the effect of coating thickness. Chromel-alumel thermocouples were used to provide data up to 2500°F. The data from each test are shown in Figure 26. The typical configuration of the nozzle assembly is also shown in Figure 26. Each nozzle was of the same size and was insulated from the steel housing with a machined carbon sleeve. This arrangement reduces the heat sink effect of the steel housing and allows the exposed nozzle surface to rapidly heat to a realistically high temperature. No attempt was made to measure temperatures at the coating itself since such an attempt might seriously compromise the serviceability of the coating. The location at the back of the coated section where temperature data were taken probably represents about the average temperature in the substrate which is protected by the pyrolytic graphite surface coating.

The decrease in the rate of temperature rise in nozzles with a nominal 50 mil coating compared to nozzles with a nominal 25 mil coating is apparent for both the 6000°F and 6500°F propellant firings. Also, the more rapid temperature rise anticipated with the hotter propellant is well documented. The low thermal conductivity of the pyrolytic graphite coating is responsible for the substantial time required to reach 2500°F in the nozzle substrate material. The surface temperature of a nozzle coated with such an insulating material approaches the gas temperature very rapidly, however. It is possible to calculate the surface temperature of a coated nozzle, even though the direct measurement of this temperature was not attempted. The surface temperature was calculated using a simplified analysis of the heat transfer in the nozzle under conditions similar to those of firing PYC-4; the calculated curve is included in Figure 26. Within about 5 seconds the surface temperature is calculated to rise to within a few hundred degrees of the gas temperature (local free stream temperature of about 5600°F for this propellant). The insulating characteristics of pyrolytic

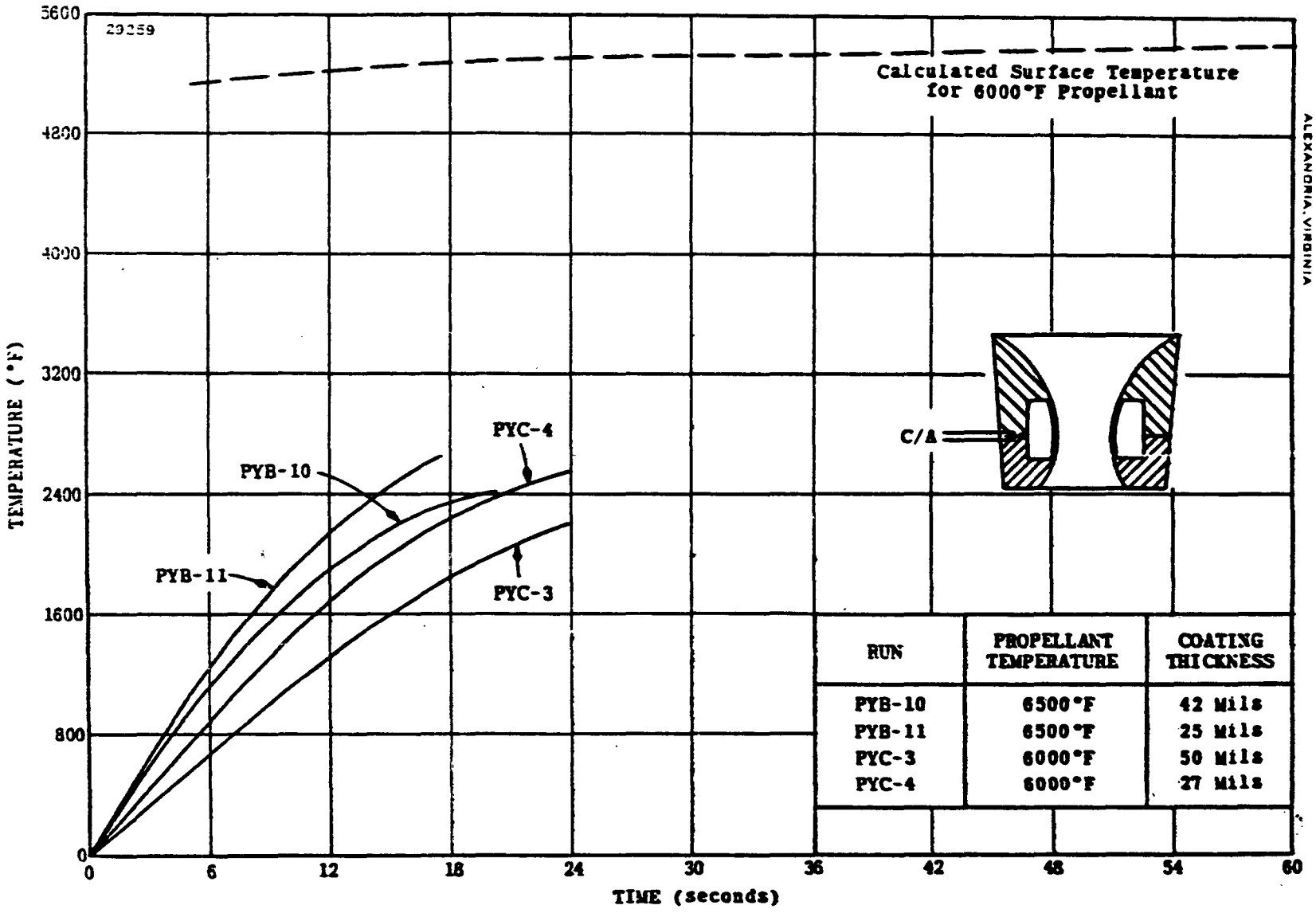

Figure 26. Nozzle Temperatures During Rocket Motor Firings.

graphite causes the surface temperature to exceed that reached by a more conductive heat sink nozzle. In spite of this higher surface temperature, pyrolytic graphite is more erosion resistant than the other forms of graphite.

6. One-Inch Diameter Nozzle Tests

As a beginning in the scale-up of pyrolytic graphite nozzles two highly successful firings were made with one inch diameter nozzles. These tests were made with the 6000°F propellant formulated with an oxidation ratio of 1.20. This propellant was selected because it provides severe test conditions characteristic of many advanced rocket motor designs. The use of an oxidizer-rich formulation assured that the oxidation sensitivity of pyrolytic graphite was critically evaluated.

The nozzles tested consisted of a three-piece segmented design. The section coated with the standard (2000°C) pyrolytic graphite extended upstream from the throat to the point where the area was twice that of the throat. The entrance and exit segments of the nozzle were machined from high density (Grade ZTA) molded graphite. The conditions and results of each firing test are included in Table VIII.

In the first test (PYC-7) an erosion rate of 0.54 mil/sec was measured at an average motor pressure of 1167 psi and a firing duration of 29.9 seconds. The erosion rate predicted from sub-scale tests with one-half inch nozzles is 0.49 mil/sec which is in excellent agreement with the observed value. This test actually represents an extrapolation to a higher motor pressure than with the smaller nozzles and was a very severe test indeed. The excellent performance of the pyrolytic graphite was obtained in spite of substantial erosion of the inlet section of high density graphite which exposed the entire leading edge of the coating during the firing.

In the second test (PYC-8) an average motor pressure of 829 psi was achieved for a firing duration of 55.7 seconds. This pressure level is more representative of common design practice. The measured erosion rate of the pyrolytic graphite nozzle was 0.42 mil/sec. This is good performance although the predicted erosion rate from sub-scale tests would be only about half this value. The erosion of the entrance high density graphite section was excessive in this test with the entire cross-section of the coated throat piece being exposed at the end of firing. Coating damage progressed some distance from the

upstream edge but did not reach the throat region. It is clear that the ZTA molded graphite at the inlet end was inadequate for the conditions of this long duration firing. Turbulence caused by the eroded entrance section probably caused increased erosion of the coating. The fact that the coating survived under this adverse condition is significant. The photograph of this nozzle after test, shown in Figure 27 clearly shows the erosion of the high density graphite entrance cap and the limited damage to the pyrolytic graphite coating at the converging section. The entrance cap should be improved for further larger scale tests but the fact that a pyrolytic graphite coating can survive severe edge exposure adds assurance that satisfactory scale-up is possible.

D. DESIGN OF TWO-INCH DIAMETER NOZZLE

The successful firing of two nozzles of one inch diameter proved the capability of pyrolytic graphite to perform satisfactorily at that size level. The next objective then became the further scale-up to demonstrate serviceability at two inch nozzle diameter. Even though no funds were available for motor tests, it was agreed that preliminary nozzle design work should be carried out.

Several segmented designs were considered for the two-inch nozzle. It was apparent that an improvement in the quality of the material in the entrance cap would be required if reliable performance of a pyrolytic graphite insert was to be assured. Several approaches are apparent, but no firm decision was made on the entrance cap since test firings were not of immediate concern. Rather, the coated insert contour was selected and suitable substrate pieces designed. A good quality coating prepared on a two inch diameter nozzle is shown in Figure 28.

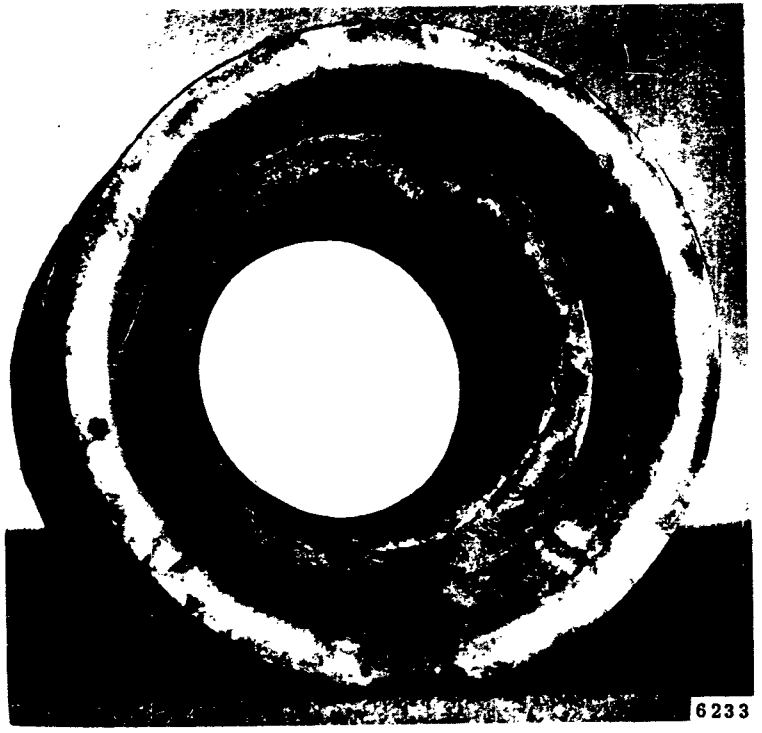

Entrance View

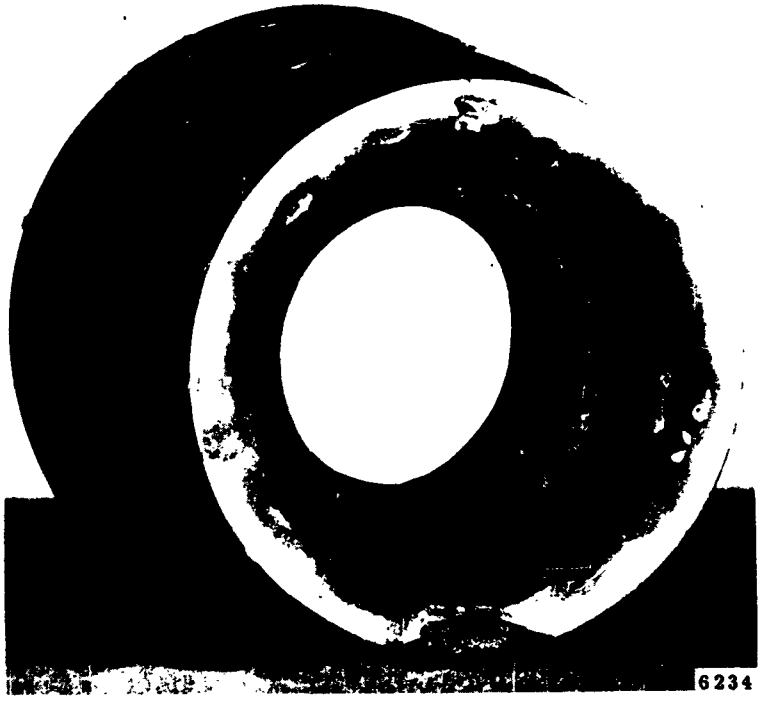

Exit View

Figure 27. Segmented One-Inch Nozzle After Full Duration Test (PYC-8)

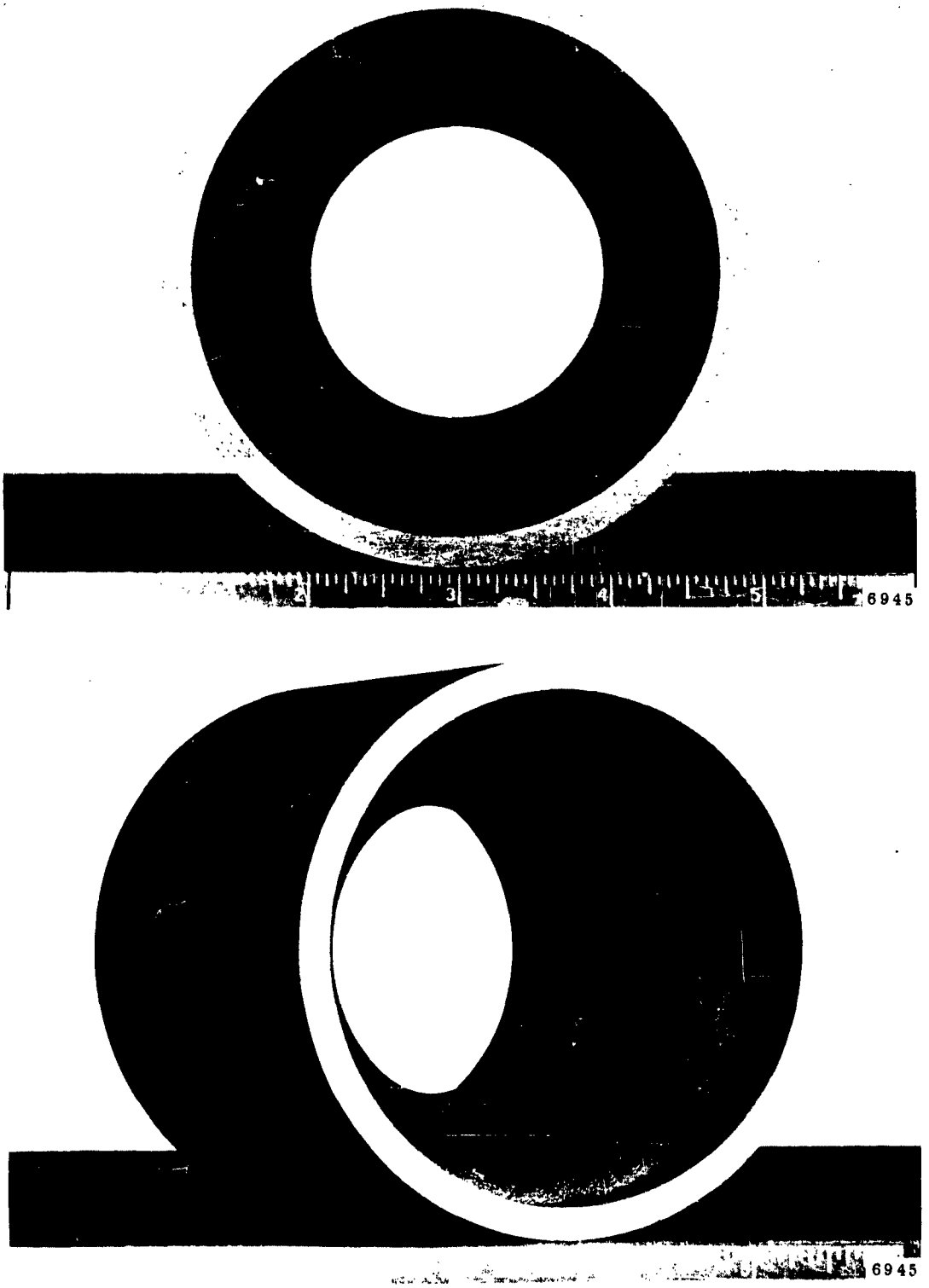

Figure 28. Pyrolytic Graphite Coated Segment for Two-Inch Nozzle.

VI. MECHANICAL DESIGN ANALYSES

In the early portion of this program, the effect of elastic anisotropy (i.e., two different moduli of elasticity, one perpendicular and one parallel to the surface) on the maximum stress in a cylinder under axisymmetric load was estimated. This analysis indicated that for a modulus ratio of 1.6 about a 30 per cent augmentation in the maximum stress occurred. Further consideration indicated that the assumptions of this analysis were very restrictive and that, indeed, for a thin, free-standing shell of an anisotropic material, no increased stress would occur. Since this would not be true for a thick shell or for a supported shell of an anisotropic material, it appeared advantageous to derive more exact stress analyses for pyrolytic graphite shells.

An acceptable mechanical design for a pyrolytic graphite nozzle must be one in which the stresses in the nozzle do not exceed the strength of the materials. The stresses which appear in a pyrolytic graphite structure may be categorized into three groups as follows:

(1) Residual stresses produced in manufacture,

(2) Pressurization stresses produced in service, and

(3) Thermal stresses in service produced by transient temperature gradients.

The stresses in (1) above arise because of the unequal thermal contraction of pyrolytic graphite in its a-direction and c-direction during cooling from the deposition temperature and from mismatch of expansion coefficients between the substrate and coating. The calculation of these stresses is complicated by the elastic anisotropy of the material. The residual stresses from manufacture for a pyrolytic graphite coating on a substrate will be different from those in a free-standing shell of pyrolytic graphite, but the stresses will not vanish in either case. The stresses in groups (2) and (3) are caused by using the material in a rocket motor environment. The stresses in group (3) can be significant since the low thermal conductivity of pyrolytic graphite in its c-direction leads to very large thermal gradients across the thickness of the pyrolytic graphite shell.

A. STRESS-STRAIN RELATIONS FOR PYROLYTIC GRAPHITE

In the following mathematical analysis, the general stress-strain relations for a material which exhibits the particular form of anisotropy found in pyrolytic graphite are derived. Simplifying assumptions are avoided so that general applicability can be maintained. In later sections, the more tractable cases of simplified form are considered to derive practical conclusions within the limited scope of the analysis phase of this program. However, the derivations in this section appear to be of sufficient importance as background to be included here.

Pyrolytic graphite, which exhibits a limited form of anisotropy, is better described as a "transversely isotropic" material, i.e., all directions parallel to the deposit plane are elastically equivalent. It can be shown that the energy stored per unit volume of such a material is given in terms of the local strains by an expression involving five independent constants. Taking a rectangular coordinate system with the y-axis perpendicular to the deposit plant, this "strain-energy function" may be written as

$$W = \frac{C_{11}}{2}(\epsilon_x^2 + \epsilon_z^2) + \frac{C_{22}}{2}\epsilon_y^2 + C_{12}(\epsilon_x \epsilon_y + \epsilon_y \epsilon_z)$$

$$+ C_{13}\epsilon_x \epsilon_z + \frac{C_{44}}{2}(\gamma_{xy}^2 + \gamma_{yz}^2) + \frac{C_{11} - C_{13}}{4}\gamma_{zx}^2 \qquad (1)$$

where the C's are constants, the ϵ's are normal strains, and the γ's are shear strains. The nomenclature is standard engineering notation such as that described by Timoshenko. The stress-strain relations for such a material may be found from (1) by partial differentiation:

$$\frac{\partial W}{\partial \epsilon_x} = \sigma_x = C_{11}\epsilon_x + C_{12}\epsilon_y + C_{13}\epsilon_z \qquad (2.1)$$

$$\frac{\partial W}{\partial \epsilon_y} = \sigma_y = C_{12}\epsilon_x + C_{22}\epsilon_y + C_{12}\epsilon_z \qquad (2.2)$$

$$\frac{\partial W}{\partial \epsilon_z} = \sigma_z = C_{13}\epsilon_x + C_{12}\epsilon_y + C_{11}\epsilon_z \qquad (2.3)$$

$$\frac{\partial W}{\partial \gamma_{xy}} = \tau_{xy} = C_{44}\gamma_{xy} \qquad (2.4)$$

$$\frac{\partial W}{\partial \gamma_{yz}} = \tau_{yz} = C_{44}\gamma_{yz} \tag{2.5}$$

$$\frac{\partial W}{\partial \gamma_{zx}} = \tau_{zx} = \frac{C_{11} - C_{13}}{2}\gamma_{zx} \tag{2.6}$$

where the σ's are normal stresses and the τ's are shear stresses.

The strain-stress relations may also be written in terms of seven "engineering" elastic moduli:

$$\epsilon_x = \frac{1}{E_{\parallel}}\sigma_x - \frac{\nu_1}{E_{\perp}}\sigma_y - \frac{\nu_3}{E_{\parallel}}\sigma_z \tag{3.1}$$

$$\epsilon_y = -\frac{\nu_2}{E_{\parallel}}\sigma_x + \frac{1}{E_{\perp}}\sigma_y - \frac{\nu_2}{E_{\parallel}}\sigma_z \tag{3.2}$$

$$\epsilon_z = -\frac{\nu_3}{E_{\parallel}}\sigma_x - \frac{\nu_1}{E_{\perp}}\sigma_y + \frac{1}{E_{\parallel}}\sigma_z \tag{3.3}$$

$$\gamma_{xy} = \frac{\tau_{xy}}{G_{\perp}} \tag{3.4}$$

$$\gamma_{yz} = \frac{\tau_{yz}}{G_{\perp}} \tag{3.5}$$

$$\gamma_{zx} = \frac{\tau_{zx}}{G_{\parallel}} \tag{3.6}$$

where the ν's are Poisson's ratios, the E's are Young's moduli, and the G's are moduli of rigidity. The subscript $\parallel$ refers to the plane parallel to the coating surface (a-direction in pyrolytic graphite terminology); the subscript $\perp$ refers to the axis perpendicular to the coating surface (c-direction). Only five of the engineering moduli are independent, since it can be deduced from the equations (2) that

$$\frac{\nu_1}{E_{\perp}} = \frac{\nu_2}{E_{\parallel}} \tag{4.1}$$

$$G_{\parallel} = \frac{E_{\parallel}}{2(1 + \nu_3)} \tag{4.2}$$

The engineering moduli are given in terms of the C's by the relations

$$E_{\parallel} = (C_{11} - C_{13})\left(1 + \frac{C_{13}C_{22} - C_{12}^2}{C_{11}C_{22} - C_{12}^2}\right) \tag{5.1}$$

$$E_{\perp} = C_{22} - 2\frac{C_{12}^2}{C_{11} + C_{13}} \tag{5.2}$$

$$\nu_1 = \frac{C_{12}}{C_{11} + C_{13}} \tag{5.3}$$

$$\nu_2 = \frac{C_{12}(C_{11} - C_{13})}{C_{11}C_{22} - C_{12}^2} \tag{5.4}$$

$$\nu_3 = \frac{C_{13}C_{22} - C_{12}^2}{C_{11}C_{22} - C_{12}^2} \tag{5.5}$$

$$G_{\parallel} = \frac{C_{11} - C_{13}}{2} \tag{5.6}$$

$$G_{\perp} = C_{44} \tag{5.7}$$

The C's are given in terms of the engineering moduli by

$$C_{11} = \frac{E_{\parallel}}{1 + \nu_3}\,\frac{1 - \nu_1\nu_2}{1 - 2\nu_1\nu_2 - \nu_3} \tag{6.1}$$

$$C_{12} = \frac{\nu_1 E_{\parallel}}{1 - 2\nu_1\nu_2 - \nu_3} \tag{6.2}$$

$$C_{13} = \frac{E_{\parallel}}{1 + \nu_3}\,\frac{\nu_1\nu_2 + \nu_3}{1 - 2\nu_1\nu_2 - \nu_3} \tag{6.3}$$

$$C_{22} = \frac{\nu_1 (1 - \nu_3) E_{\parallel}}{\nu_2 (1 - 2\nu_1\nu_2 - \nu_3)} \tag{6.4}$$

$$C_{44} = G_{\perp} \tag{6.5}$$

The condition that the strain-energy function (1) must always be positive or zero leads to a set of inequalities which must be satisfied by the C's:

$$C_{11} \geq 0 \tag{7.1}$$

$$C_{11} \geq C_{13} \geq - C_{11} \tag{7.2}$$

$$C_{22}(C_{11} + C_{13}) - 2C_{12}^{2} \geq 0 \tag{7.3}$$

$$C_{44} \geq 0 \tag{7.4}$$

The corresponding inequalities for the engineering modul are

$$E_{\parallel} \geq 0 \tag{8.1}$$

$$E_{\perp} \geq 0 \tag{8.2}$$

$$G_{\parallel} \geq 0 \tag{8.3}$$

$$G_{\perp} \geq 0 \tag{8.4}$$

$$1 \geq \nu_3 \geq - 1 \tag{8.5}$$

$$1 - 2\nu_1\nu_2 - \nu_3 \geq 0 \tag{8.6}$$

If thermal expansion effects are important, the equations (3) must be rewritten as

$$\epsilon_x = \frac{\sigma_x}{E_{\parallel}} - \frac{\nu_1}{E_{\perp}} \sigma_y - \frac{\nu_3}{E_{\parallel}} \sigma_z + A_{\parallel}(T) \tag{9.1}$$

$$\epsilon_y = -\frac{\nu_2}{E_{\parallel}}\sigma_x + \frac{\sigma_y}{E_{\perp}} - \frac{\nu_2}{E_{\parallel}}\sigma_z + A_{\perp}(T) \tag{9.2}$$

$$\epsilon_z = -\frac{\nu_3}{E_{\parallel}}\sigma_x - \frac{\nu_1}{E_{\perp}}\sigma_y + \frac{\sigma_z}{E_{\parallel}} + A_{\parallel}(T) \tag{9.3}$$

$$\gamma_{xy} = \frac{\tau_{xy}}{G_{\perp}} \tag{9.4}$$

$$\gamma_{yz} = \frac{\tau_{yz}}{G_{\perp}} \tag{9.5}$$

$$\gamma_{zx} = \frac{\tau_{zx}}{G_{\parallel}} \tag{9.6}$$

$$\text{where } A_{\parallel}(T) = \int_{T_o}^{T} \alpha_{\parallel}(T)\, dT, \tag{10.1}$$

$$A_{\perp}(T) = \int_{T_o}^{T} \alpha_{\perp}(T)\, dT. \tag{10.2}$$

Here $\alpha_{\parallel}$ and $\alpha_{\perp}$ are the thermal expansion coefficients of the material in directions respectively parallel to, and perpendicular to the deposit plane.

In the case of pyrolytic graphite, "T_o" must be interpreted as a temperature at which the material is free of internal thermal stresses, e.g. the deposition temperature.

When the equations (3) are similarly modified to include the effects of thermal expansion, the results are

$$\sigma_x = C_{11}\epsilon_x + C_{12}\epsilon_y + C_{13}\epsilon_z - B_1(T) \tag{11.1}$$

$$\sigma_y = C_{12}\epsilon_x = C_{22}\epsilon_y + C_{12}\epsilon_z - B_2(T) \tag{11.2}$$

$$\sigma_z = C_{13}\epsilon_x + C_{12}\epsilon_y + C_{11}\epsilon_z - B_1(T) \tag{11.3}$$

$$\tau_{xy} = C_{44}\gamma_{xy} \tag{11.4}$$

$$\tau_{yz} = C_{44}\gamma_{yz} \tag{11.5}$$

$$\tau_{zx} = \frac{C_{11} - C_{13}}{2}\gamma_{zx} \tag{11.6}$$

where

$$B_1(T) = (C_{11} + C_{13})A_{\parallel}(T) + C_{12}A_{\perp}(T) \tag{12.1}$$

$$B_2(T) = 2C_{12}A_{\parallel}(T) + C_{22}A_{\perp}(T) \tag{12.2}$$

B. STRESSES IN A HOLLOW CYLINDER OF PYROLYTIC GRAPHITE

The stress-strain relations derived above (Equations 11) must be converted to the cylindrical coordinate system (r, θ, z). Since pyrolytic graphite coatings form with the layer planes (a-direction) parallel to the substrate surface, the axis of elastic symmetry (c-direction) of the pyrolytic graphite is radially directed. In cylindrical coordinates the equations (11) become:

$$\sigma_\theta = C_{11}\epsilon_\theta + C_{12}\epsilon_r + C_{13}\epsilon_z - B_1(T) \tag{13.1}$$

$$\sigma_r = C_{12}\epsilon_\theta + C_{22}\epsilon_r + C_{12}\epsilon_z - B_2(T) \tag{13.2}$$

$$\sigma_z = C_{13}\epsilon_\theta + C_{12}\epsilon_r + C_{11}\epsilon_z - B_1(T) \tag{13.3}$$

$$\tau_{r\theta} = C_{44}\gamma_{r\theta} \tag{13.4}$$

$$\tau_{rz} = C_{44}\gamma_{rz} \tag{13.5}$$

$$\tau_{\theta z} = \frac{C_{11} - C_{13}}{2}\gamma_{\theta z} \tag{13.6}$$

The cylinder is assumed to be of finte length 2L; the ends at $z = \pm L$ are free to move.

We will consider those stresses which arise from pressurization, unequal thermal expansion coefficients, and radial temperature

gradients. In all these cases the elastic deformation is axisymmetric, and the shearing strains $\gamma_{r\theta}$, $\gamma_{\theta z}$ vanish. From (13.4) and (13.6), the shearing stresses $\tau_{r\theta}$ and $\tau_{\theta z}$ must vanish also.

The equations of elastic equilibrium reduce to

$$\frac{\partial \sigma_r}{\partial r} + \frac{\partial \tau_{rz}}{\partial z} + \frac{\sigma_r - \sigma_\theta}{r} = 0 \tag{14.1}$$

$$\frac{\partial \tau_{rz}}{\partial r} + \frac{\partial \sigma_z}{\partial z} + \frac{\tau_{rz}}{r} = 0 \tag{14.2}$$

Now let u, v, W be the displacements of the strained elastic material parallel to the r, θ, and Z axes, respectively. Because of the axisymmetric nature of this problem, v = o. The strains ϵ_r, ϵ_θ, ϵ_z, γ_{rz} are connected with the displacements u, W, by the equations

$$\epsilon_r = \frac{\partial u}{\partial r} \tag{15.1}$$

$$\epsilon_\theta = \frac{u}{r} \tag{15.2}$$

$$\epsilon_z = \frac{\partial W}{\partial z} \tag{15.3}$$

$$\gamma_{rz} = \frac{\partial u}{\partial z} + \frac{\partial W}{\partial r} \tag{15.4}$$

By using the stress-strain equations (13), the stresses can be expressed in terms of the displacements as

$$\sigma_\theta = C_{11}\frac{u}{r} + C_{12}\frac{\partial u}{\partial r} + C_{13}\frac{\partial W}{\partial z} - B_1(r) \tag{16.1}$$

$$\sigma_r = C_{12}\frac{u}{r} + C_{22}\frac{\partial u}{\partial r} + C_{12}\frac{\partial W}{\partial z} - B_2(r) \tag{16.2}$$

$$\sigma_z = C_{13}\frac{u}{r} + C_{12}\frac{\partial u}{\partial r} + C_{11}\frac{\partial W}{\partial z} - B_1(r) \tag{16.3}$$

$$\tau_{rz} = C_{44}\left(\frac{\partial u}{\partial z} + \frac{\partial W}{\partial r}\right) \tag{16.4}$$

(Here $B_1(r)$ and $B_2(r)$ have been written instead of $B_1[T(r)]$ and $B_2[T(r)]$.) Putting these relations into the equilibrium equations (14), we find

$$C_{22}\left(\frac{\partial^2 u}{\partial r^2} + \frac{1}{r}\frac{\partial u}{\partial r}\right) + C_{44}\frac{\partial^2 u}{\partial z^2} + (C_{12} + C_{44})\frac{\partial^2 W}{\partial r \partial z} - C_{11}\frac{u}{r^2}$$

$$+ (C_{12} - C_{13})\frac{1}{r}\frac{\partial W}{\partial z} = \frac{B_2 - B_1}{r} + \frac{\partial B_2}{\partial r} \tag{17.1}$$

and

$$(C_{12} + C_{44})\frac{\partial^2 u}{\partial r \partial z} + (C_{13} + C_{44})\frac{1}{r}\frac{\partial u}{\partial z} + C_{44}\left(\frac{\partial^2 W}{\partial r^2} + \frac{1}{r}\frac{\partial W}{\partial r}\right)$$

$$+ C_{11}\frac{\partial^2 W}{\partial z^2} = 0 \tag{17.2}$$

We must solve the equations (17.1) and (17.2) with the boundary conditions

$$\sigma_r = P_i,\ \tau_{rz} = 0 \qquad \text{at} \qquad r = R_i$$

$$\sigma_r = P_o,\ \tau_{rz} = 0 \qquad \text{at} \qquad r = R_o$$

$$\sigma_z = \tau_{rz} = 0 \qquad \text{at} \qquad z = \pm L$$

Here P_i and P_o are the inside and outside pressures and R_i and R_o are the inside and outside radii, respectively.

The solution $u(r,z)$, $W(r,z)$ of the equations (17), (18) can be made to depend on the solutions of two simpler problems:

Problem "A"

Solve the equations (17) in an infinitely long cylinder with the boundary conditions $\sigma_r = P_i,\ \tau_{rz} = 0$ at $r = R_i$ (19.1)

$$\sigma_r = P_o, \ \tau_{rz} = 0 \ \text{ at } r = R_o \qquad (19.2)$$

and subject to the restriction that $\int_{R_i}^{R_o} \sigma_z r dr = 0$ (19.3)

Denote the displacements and stresses obtained by the subscript "A", i.e. u_A, W_A, σ_{r_A}, etc.

Problem "B"

Solve the equations (17), without the thermal stress terms which appear on the right hand side of (17.1), in a semi-infinite cylinder with the boundary conditions $\sigma_r = \tau_{rz} = 0$ at $r = R_i$ (20.1)

$$\sigma_r = \tau_{rz} = 0 \ \text{ at } \ r = R_o \qquad (20.2)$$

$$\sigma_z = F(r), \ \tau_{rz} = G(r) \text{ at } z = 0 \qquad (20.3)$$

The function $F(r)$, which gives the distribution of normal forces over the end of the cylinder, is subject to the condition that

$$\int_{R_i}^{R_o} F(r)\, r dr = 0, \text{ i.e. these forces must} \qquad (20.4)$$

be self-equilibrating. In obtaining the stresses σ_θ, σ_r, σ_z, τ_{rz} omit the thermal stress terms $B_1(T)$, $B_2(T)$ in (16.1), (16.2), (16.3). Denote the displacements and stresses obtained by the subscript "B".

If both problems "A" and "B" have been solved, the solution u, W of the original problem (17), (18) may be obtained as follows:

Apply the formulae for problem "B" with $F(r) = -\sigma_{z_A}$, $G(r) = 0$. Call the resulting displacements and stresses ${}_1u_B$, ${}_1W_B$, ${}_1\sigma_{r_B}$, etc.

Apply the formulae for problem "B" with $F(r) = -\left[{}_1\sigma_{z_B}\right]_{z = 2L}$, $G(r) = -\left[{}_1\tau_{rz_B}\right]_{z = 2L}$. Call the resulting displacements and stresses ${}_2u_B$, ${}_2W_B$, ${}_2\sigma_{r_B}$, etc.

Apply the formulae for problem "B" with $F(r) = -\left[{}_2\sigma_{z_B}\right]_{z = 2L}$, $G(r) = -\left[{}_2\tau_{rz_B}\right]_{z = 2L}$. Call the resulting displacements and stresses ${}_3u_B$, ${}_3W_B$, ${}_3\sigma_{r_B}$, etc.

And so forth - - -

The solution of the original problem can now be written as

$$u = u_A(r) + {}_1u_B(r, L - z) + {}_2u_B(r, L - z) + \ldots + {}_1u_B(r, L + z) + {}_2u_B(r, L + z) + \qquad (21.1)$$

$$W = W_A(r_1 z) + {}_1W_B(r, L - Z) + {}_2W_B(r, L - z) + \ldots + {}_1W_B(r, L + z) + {}_2W_B(r, L + z) + \ldots \qquad (21.2)$$

$$\sigma_r = \sigma_{r_A}(r) + {}_1\sigma_{r_B}(r, L - z) + {}_2\sigma_{r_B}(r, L - z) + \ldots + {}_1\sigma_{r_B}(r, L + z) + {}_2\sigma_{r_B}(r, L + z) + \ldots \qquad (21.3)$$

and so forth .....

The series (21) should converge rapidly if the ratio $\frac{R_o - R_i}{L}$ of the cylinder wall thickness to the cylinder half-length is small.

A similar image superposition procedure will reduce any problem involving single or composite elastic solids of revolution to a problem of type "A", dealing with the response of an infinite solid to pressurization and thermal stresses, and problems of type "B", dealing with the response of a semi-infinite solid to self-equilibriating normal stresses and tractions applied to the end surface.

It should be noted that the equations (17) can be used to calculate transient thermal stresses only if the elastic constants

C_{11}, C_{12}, C_{13}, C_{22}, C_{44} are independent of temperature for the temperature range being considered. If this is not the case, additional terms appear in the equations (17). The reduction to problems of the types "A" and "B" can still be carried out, but the type "B" equations are no longer free of thermal stress terms.

We will now consider the problem "A" for a hollow cylinder of transversely isotropic material, making the assumption that the elastic constants are independent of temperature:

Since the cylinder is infinitely long,

$$\frac{\partial \sigma_r}{\partial z} = \frac{\partial \sigma_\theta}{\partial z} = \frac{\partial \sigma_z}{\partial z} = 0, \quad \tau_{rz} = \gamma_{rz} = 0, \quad \text{and} \quad \frac{\partial \epsilon_r}{\partial z} = \frac{\partial \epsilon_\theta}{\partial z} = \frac{\partial u}{\partial z} = 0,$$

Moreover, the cylinder is in a state of constant axial strain; i.e. $\epsilon_z = \frac{\partial W}{\partial z} = K$ (a constant), and $\frac{\partial W}{\partial r} = 0$. (These results hold for multi-layer, composite cylinders also.)

The second equilibrium equation (17.2) is satisfied identically. The first equilibrium equation (17.1) reduces to

$$\frac{d^2u}{dr^2} + \frac{1}{r}\frac{du}{dr} - \frac{C_{11}}{C_{22}}\frac{u}{r^2} = \frac{B_2(r) - B_1(r) - K(C_{12} - C_{13})}{C_{22}r} + \frac{1}{C_{22}}\frac{dB_2}{dr} \tag{22.1}$$

Using the relations (16), the boundary conditions (19.1), (19.2) reduce to

$$\sigma_r = C_{12}\frac{u}{R_i} + C_{22}\frac{du}{dr} + C_{12}K - B_2(R_i) = P_i \text{ at } r = R_i \tag{22.2}$$

$$\sigma_r = C_{12}\frac{u}{R_o} + C_{22}\frac{du}{dr} + C_{12}K - B_2(R_o) = P_o \text{ at } r = R_o \tag{22.3}$$

Finally, the condition (19.3) becomes

$$\int_{R_i}^{R_o} \sigma_z r dr = \int_{R_i}^{R_o} \left[C_{13} \frac{u}{r} + C_{12} \frac{du}{dr} + C_{11} K - B_1 (r) \right] r dr = 0 \quad (22.4)$$

This last condition (22.4) will determine the constant K. The general solution of the equation (22.1) is of the form

$$u = \frac{C_{13} - C_{12}}{C_{22} - C_{11}} Kr + A_1 r^{\gamma} + A_2 r^{-\gamma}$$
$$+ \frac{r^{\gamma}}{C_{22}} \int_{R_i}^{r} r^{-1-2\gamma} \int_{R_i}^{r} \left[\frac{R_2(r) - B_1(r)}{r} + \frac{dB_2}{dr} \right] r^{1+\gamma} \, drdr. \quad (23)$$

where A_1 and A_2 are arbitrary constants, and $\gamma = \frac{C_{11}}{C_{22}}$. (24)

We will consider only the case in which the cylinder is at a uniform temperature. The general solution of (22.1) is then

$$u = \frac{C_{13} - C_{12}}{C_{22} - C_{11}} Kv + \frac{B_2 - B_1}{C_{22} - C_{11}} r + A_1 r^{\gamma} + A_2 r^{-\gamma}. \quad (25)$$

When this expression is substituted into the boundary conditions (22.2), (22.3) and into the equilibrium condition (22.4), three simultaneous equations are found which must be solved for the three unknowns K, A_1, A_2. These equations may be written as

$$F_{11} K + F_{12} A_1 + F_{13} A_2 = G_1 \quad (26.1)$$

$$F_{21} K + F_{22} A_1 + F_{23} A_2 = G_2 \quad (26.2)$$

$$F_{31} K + F_{32} A_1 + F_{33} A_2 = G_3 \quad (26.3)$$

with

$$F_{11} = C_{12} + \frac{C_{13} - C_{12}}{C_{22} - C_{11}} (C_{12} + C_{22}) \quad (27.1)$$

$$F_{12} = (C_{12} + \gamma C_{22}) R_1^{\gamma - 1} \quad (27.2)$$

$$F_{13} = (C_{12} - \gamma C_{22})\, R_i^{-\gamma - 1} \tag{27.3}$$

$$G_1 = P_i + B_2 - \frac{C_{12} + C_{22}}{C_{22} - C_{11}} (B_2 - B_1) \tag{27.4}$$

$$F_{21} = C_{12} + \frac{C_{13} - C_{12}}{C_{22} - C_{11}} (C_{12} + C_{22}) \tag{27.5}$$

$$F_{22} = (C_{12} + \gamma C_{22})\, R_o^{\gamma - 1} \tag{27.6}$$

$$F_{23} = (C_{12} - \gamma C_{22})\, R_o^{-\gamma - 1} \tag{27.7}$$

$$G_2 = P_o + B_2 - \frac{C_{12} + C_{22}}{C_{22} - C_{11}} (B_2 - B_1) \tag{27.8}$$

$$F_{31} = \left(\frac{C_{13}^2 - C_{12}^2}{C_{22} - C_{11}} + C_{11} \right) \frac{R_o^2 - R_i^2}{2} \tag{27.9}$$

$$F_{32} = (C_{13} + \gamma C_{12}) \frac{R_o^{1 + \gamma} - R_i^{1 + \gamma}}{1 + \gamma} \tag{27.10}$$

$$F_{33} = (C_{13} - \gamma C_{12}) \frac{R_o^{1 - \gamma} - R_i^{1 - \gamma}}{1 - \gamma} \tag{27.11}$$

$$G_3 = \left[B_1 - \frac{C_{12} + C_{13}}{C_{22} - C_{11}} (B_2 - B_1) \right] \frac{R_o^2 - R_i^2}{2} \tag{27.12}$$

Substitution of the solutions K, A_1, A_2 of the equations (26) into (25) gives the final expression for the radial displacement u. The stresses in the cylinder can then be found from the equations (16):

$$\sigma_r = F_{11}K + P_i - G_1 + (C_{12} + \gamma C_{22}) A_1 r^{\gamma - 1} + (C_{12} - \gamma C_{22}) A_2 r^{-\gamma - 1} \tag{28}$$

$$\sigma_\theta = F_{11}K + P_i - G_1 + (C_{11} + \gamma C_{12}) A_1 r^{\gamma - 1} + (C_{11} - \gamma C_{12}) A_2 r^{-\gamma - 1} \tag{29}$$

$$\sigma_z = \frac{2}{R_o^2 - R_i^2} (F_{31}K - G_3) + (C_{13} + \gamma C_{12}) A_1 r^{\gamma - 1} + (C_{13} - \gamma C_{12}) A_2 r^{-\gamma - 1} \tag{30}$$

The stresses in a cylinder of finite length will consist of "Problem A" stresses in the center such as those calculated from equations (28), (29), and (30), plus the additional stresses of the "Problem B" type near the ends of the cylinder. In particular, the shearing stress τ_{rz} is zero in the center portion of such a cylinder, but may become quite large near the cylinder ends. This fact has led to the conclusion that pyrolytic graphite coatings may fail near their edges. However, the rigorous evaluation of this effect depends on the development of methods for the solution of problems of the type "B", which are mathematically more difficult than those of type "A". Such a rigorous treatment was beyond the scope of this program, but the effect of nozzle section length on the edge stresses was of such importance as to merit further study, as outlined in the following section.

C. EFFECT OF LENGTH ON SHEAR STRESSES

Since the exact treatment of even an idealized (and simplified) composite system having the actual nozzle contour was beyond the scope of this program, a simple, logical model was examined to determine the manner in which the shearing stresses at the coating-substrate interface can be expected to vary within coated nozzles of various lengths. An axial rocket nozzle coated with pyrolytic graphite can be considered, for some purposes, as a thick composite two-component bar in which shear deformation (but no bending) is caused by the difference between the thermal expansion coefficients of the component materials. A simple approximate theory gives a reasonable picture of the distribution of interface shearing stresses in such a composite bar.

Let the composite bar have the length 2L. Let the component bars have cross-section areas A_1 and A_2, elastic moduli E_1 and E_2, and thermal expansion coefficients α_1 and α_2, respectively. Let the surface of contact between the two components have the width S.

The composite bar is free of stresses at the temperature $T = 0$. At other temperatures, differential thermal expansion causes initially plane cross-sections to become warped. Let us set up a coordinate system (x, y, z) with the x-axis parallel to the main axis of the composite bar

with the origin at the center of the bar. Let u, v, w, be displacements parallel to the x, y, and z axes, respectively. We will assume that the deformation of the composite bar can be described adequately by $u = U(x) + D(x) \cdot F(y, z)$; $v = w = 0$. Here, U (x) is a displacement parallel to the main axis of the composite bar and uniform over each cross-section of the bar; D (x) F (y, z) is a shearing distortion with an amplitude D (x) which varies along the length of the bar.

A mean interface shearing stress $\bar{\tau}$ acts across the surface of contact between the two components. $\bar{\tau}$ will be proportional to D (x);

$$\bar{\tau} = K_\tau D(x), \tag{31}$$

where K_τ is a coefficient which depends on the distortion function F (y, z). For component bar number 1, we define a "mean elongation"

$$\bar{\epsilon}_1 = K_1 \frac{\partial D}{\partial x} + \frac{\partial U}{\partial x} \tag{32}$$

(see Figure 29). Here the coefficient K_1 is chosen so that the "stress-strain" relation

$$\bar{\sigma}_1 = E_1 \bar{\epsilon}_1 - E_1 \alpha_1 T \tag{33}$$

is valid. ($\bar{\sigma}_1$ is the mean normal stress over the cross-section area, A_1.)

Similarly, we write

$$\bar{\epsilon}_2 = K_2 \frac{\partial D}{\partial x} + \frac{\partial U}{\partial x} \tag{34}$$

and

$$\bar{\sigma}_2 = E_2 \bar{\epsilon}_2 - E_2 \alpha_2 T \tag{35}$$

for component bar number 2.

If we consider the translational equilibrium in the x-direction of small sections of the component bars (Figure 30), we find

$$A_1 \frac{\partial \bar{\sigma}_1}{\partial x} + S \bar{\tau} = 0 \tag{36.1}$$

$$A_2 \frac{\partial \bar{\sigma}_2}{\partial x} - S \bar{\tau} = 0 \tag{36.2}$$

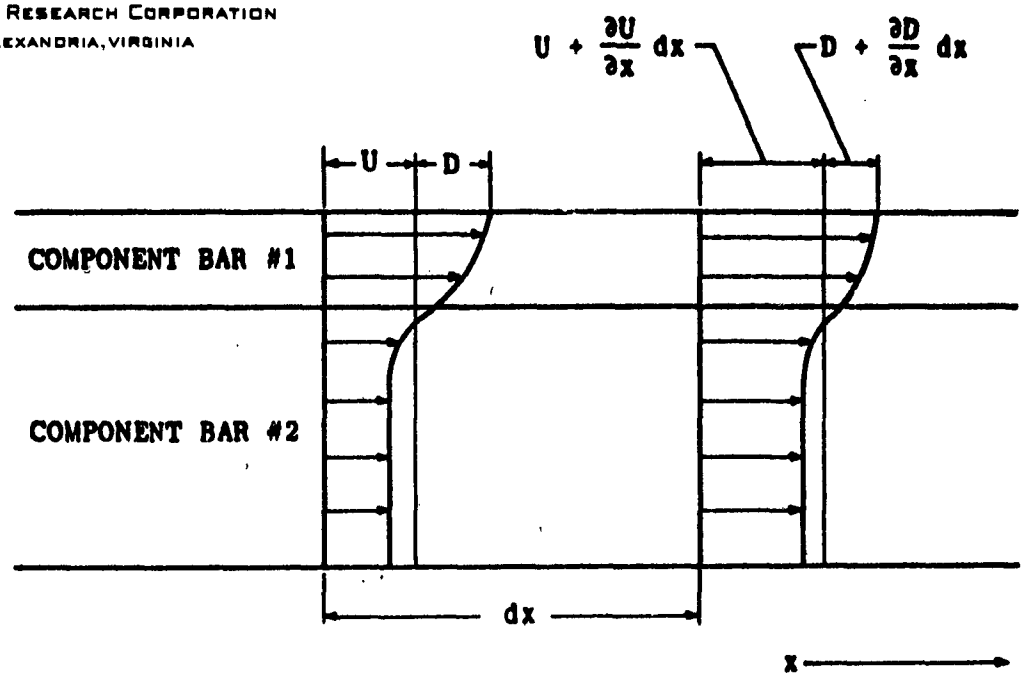

Figure 29. ELONGATION IN A COMPOSITE BAR (MODEL)

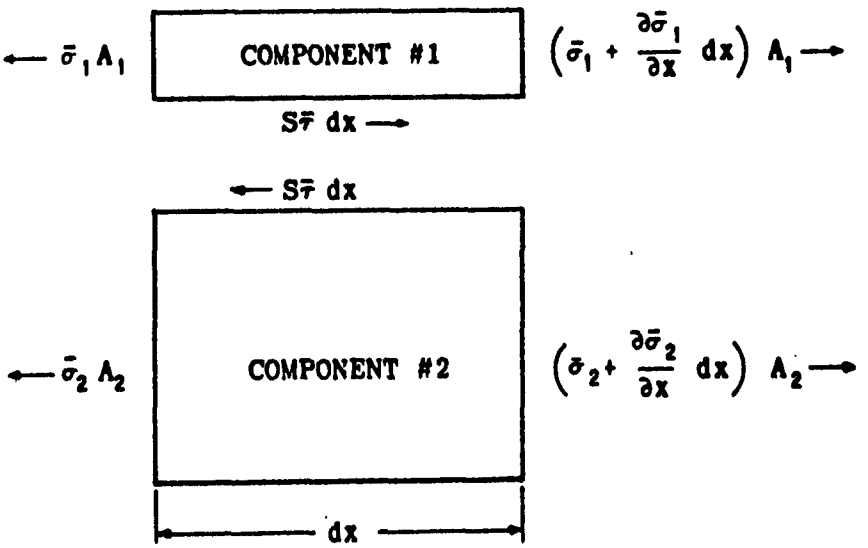

Figure 30. EQUILIBRIUM DIAGRAM FOR COMPOSITE BAR (MODEL)

Finally, since the ends of the composite bar are free, we have

$$\bar{\sigma}_1 = \bar{\sigma}_2 = 0 \quad \text{at} \quad x = \pm L. \tag{37}$$

It can easily be verified that the solution of Equations (31) - (37) is

$$D(x) = \frac{\bar{\tau}}{K_\tau} = \frac{(\alpha_2 - \alpha_1)\,T}{K_2 - K_1} \qquad \frac{\sinh \gamma x}{\gamma \cosh \gamma L} \tag{38}$$

$$U(x) = \frac{(\alpha_2-\alpha_1)T}{K_2 - K_1} \qquad \frac{\nu_1 K_2 + \nu_2 K_1}{\nu_1 + \nu_2} \qquad \frac{\sinh \gamma x}{\gamma \cosh \gamma L} + \frac{\nu_1\alpha_2 + \nu_2\alpha_1}{\nu_1 + \nu_2}\, Tx \tag{39}$$

$$\bar{\epsilon}_1 = -\nu_1 \frac{(\alpha_2 - \alpha_1)\,T}{\nu_1 + \nu_2} \qquad \frac{\cosh \gamma x}{\cosh \gamma L} + \frac{\nu_1\alpha_2 + \nu_2\alpha_1}{\nu_1 + \nu_2}\, T \tag{40.1}$$

$$\bar{\epsilon}_2 = \nu_2 \frac{(\alpha_2 - \alpha_1)\,T}{\nu_1 + \nu_2} \qquad \frac{\cosh \gamma x}{\cosh \gamma L} + \frac{\nu_1\alpha_2 + \nu_2\alpha_1}{\nu_1 + \nu_2}\, T \tag{40.2}$$

$$\bar{\sigma}_1 = \frac{E_1 \nu_1 (\alpha_2 - \alpha_1)\,T}{\nu_1 + \nu_2} \qquad \left(1 - \frac{\cosh \gamma x}{\cosh \gamma L}\right) \tag{41.1}$$

$$\bar{\sigma}_2 = \frac{E_2 \nu_2 (\alpha_2 - \alpha_1)\,T}{\nu_1 + \nu_2} \qquad \left(1 - \frac{\cosh \gamma x}{\cosh \gamma L}\right) \tag{41.2}$$

where

$$\gamma^2 = \frac{\nu_1 + \nu_2}{K_2 - K_1}$$

$$\nu_1 = \frac{SK_\tau}{A_1 E_1}$$

$$\nu_2 = \frac{SK_\tau}{A_2 E_2}$$

The dimensionless mean interface shear $\frac{\gamma (K_2 - K_1)}{K_\tau (\alpha_2 - \alpha_1) T} \bar{\tau}$ is of particular interest. In Figure 12, this quantity is plotted against dimensionless distance, γx, from the bar center for various values of the dimensionless bar half-length, γL. The sign of $\bar{\tau}$ is reversed for negative x. The dotted line is a plot of the maximum interface shear against the bar half-length.

Thus, according to this approximate theory, the maximum interface shear in a composite rocket nozzle will increase with increasing nozzle length, but will become essentially constant for sufficiently long nozzles ($\gamma L > 3/2$). For short nozzles, $\bar{\tau}$ will be proportional to distance from the nozzle center; for long nozzles, $\bar{\tau}$ will be very small in the center portion of the nozzle, but will rise exponentially as the nozzle ends are approached.

This analysis, along with considerable experimental evidence, indicates that a segmented nozzle design in which the throat section of pyrolytic graphite is relatively short should improve the reliability and serviceability of pyrolytic graphite coatings in nozzle service. The segmented nozzle concept was adopted as the standard design for the motor firings in this study. Furthermore, the scale-up effort proposed for later in this program will also be based on the use of segmented nozzles. Short coated sections will also decrease the effect of nozzle curvature, which, while not analyzed mathematically, might further accentuate edge stress concentrations.

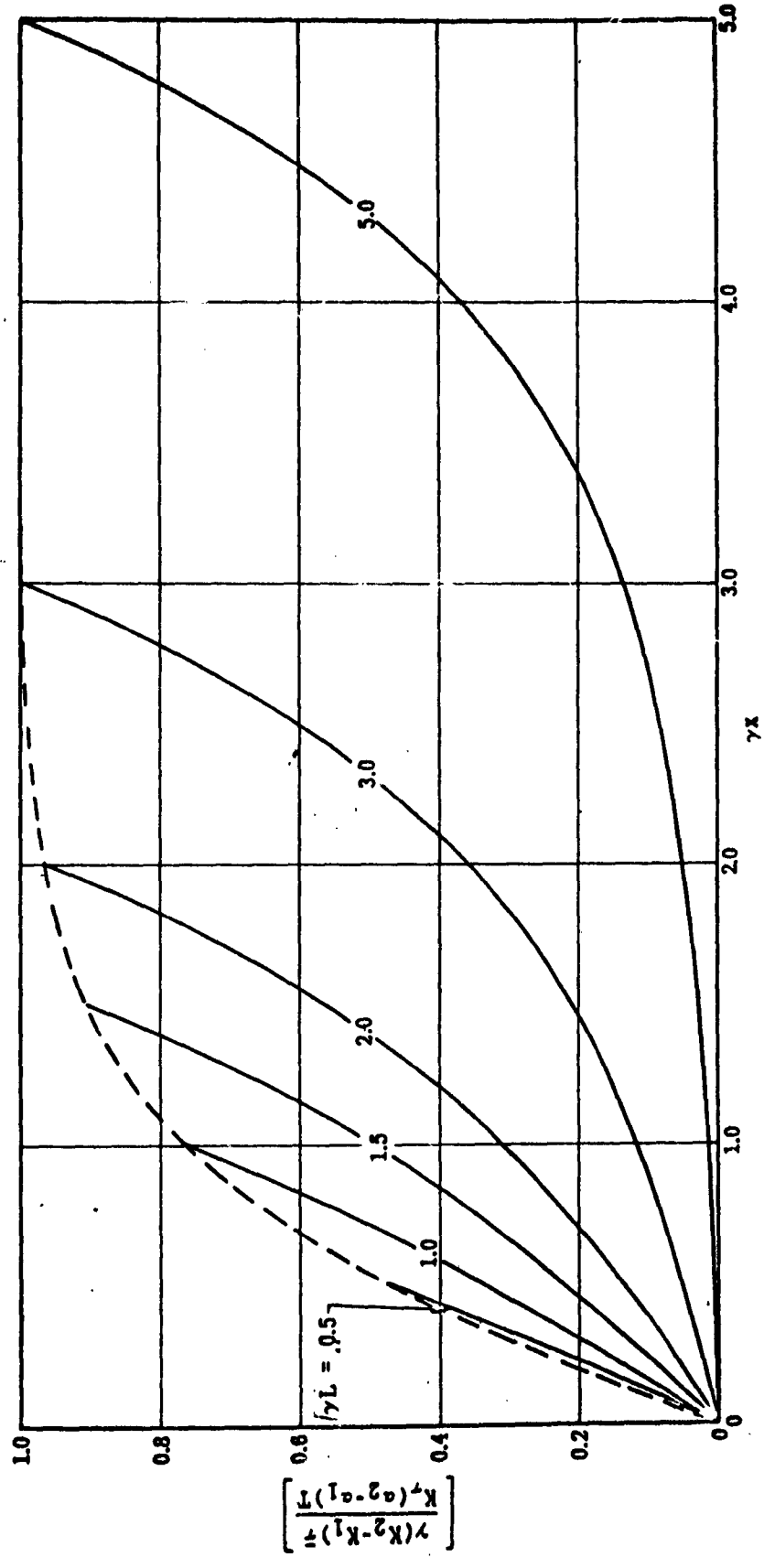

Figure 31. CALCULATED SHEAR STRESS DISTRIBUTION FOR VARIOUS LENGTH COMPOSITE BARS.

VII. SUMMARY

During the early portion of this program, the emphasis was placed on the study of the deposition process for pyrolytic graphite. A deposition technique using a cylindrical test substrate that could be sectioned for sampling and study was selected. A series of deposition runs were made to study the effect of substrate temperature, carbonaceous source gas type and concentration, and the gas dynamics on the pyrolytic graphite formed. Characterization methods used included crystalline parameter measurement by X-ray diffraction, density measurements, and extensive microscopic examination of polished sections. The microstructure of the pyrolytic graphite revealed the most about the quality of the material. Large, primary cone microstructure is generally associated with delamination cracks; a fine, regenerative microstructure is usually free of visible cracks. The X-ray measurements indicated that pyrolytic graphite forms in a turbostratic crystal structure with an interlayer d-spacing of about 3.45 Å; the crystallite dimensions in the a-direction and c-direction cover a range, but average about 120 Å and 75 Å, respectively. Density measurement indicated that the porosity of pyrolytic graphite coatings was very low. Under the conditions used in the basic process study, the rate and uniformity of the coating deposition was affected by the gas dynamics and the source gas concentration, and to a lesser extent, by the temperature.

The deposition process improvement study, which was pursued at a moderate rate of effort, was carried out in support of the nozzle preparation and testing work, and to seek methods of producing coatings of acceptable quality at reduced deposition temperatures. The nature and finish of the graphite substrate used was found to affect the surface finish of the coating, but not to have any controlling influence on the microstructure of the pyrolytic graphite deposit. Several substrate pretreatments were tested; a surface sealing process based on furane resin impregnation appeared to hold promise for reducing the population of large, coarse cones in the coating. Further work is needed to utilize this pretreatment in the preparation of low temperature deposits.

A careful study of the failure mechanisms in pyrolytic graphite nozzles was made. Examination of a series of nozzles tested previously in rocket motor firings indicated three distinct mechanisms of failure: (1) massive delamination, (2) spalling failure, and (3) erosion by chemical and mechanical means. The first two of these mechanisms can be eliminated by skill and care in the production and use of the pyrolytic graphite. The third mechanism of failure represents the true capabilities of the material on which basis materials should be judged and compared. A segmented test nozzle was designed in which the inherent capabilities of pyrolytic graphite could be accurately measured in static firings of solid propellant motors.

The mechanical design and stress analysis work included the derivation of the basic stress-strain relations for pyrolytic graphite, and the analysis of the shear stresses in coated sections. The shear stresses in coated sections, which reach a maximum near the edge, were found to be length dependent. Thus, the utility of a segmented nozzle design in which the coated throat section is kept short was demonstrated. Experimental evidence, from this program and from others, bears out the usefulness of segmented nozzles.

In the motor firing test phase, the serviceability of a standard (2000°C) pyrolytic graphite coating was determined for propellants with flame temperatures of 5600°F, 6000°F, and 6500°F. Quantitative measurements of nozzle erosion rates were made over a range of severe motor operating conditions with sub-scale motors having a nominal 0.530 inch nozzle throat diameter. In the 5600°F propellant, excellent performance was found with erosion rates of the order of 0.1 mil/sec at motor pressures near 1000 psi. Similarly, with two 6000°F propellants, the erosion rate of pyrolytic graphite was negligible below about 600 psi motor pressure and increased to about 0.4 mil/sec near 1000 psi motor pressure. In a series of motor firings with the 6500°F propellant, erosion rate was also found to be a strong function of motor pressure. At 300 psi, the erosion rate was negligible; this rate increased with increasing pressure to about 0.5 mil/sec at about 900 psi.

VIII. CONCLUSIONS AND RECOMMENDATIONS

Of the many refractory materials considered for nozzle service in solid propellant rocket motors, none has greater appeal than graphite. Many of the properties of graphite are nearly ideal for the high temperature conditions characteristic of the uncooled nozzles used in solid propellant motors. Pyrolytic graphite, which is a unique form of graphite, has been shown to have excellent erosion resistance in solid propellant rocket nozzles. The high density (essentially zero porosity) and the absence of binder phase in this material are believed to explain its serviceability which is superior to that of any other low density nozzle material known.

The sub-scale rocket motor tests carried out on a standard (2000°C) grade of pyrolytic graphite coating prepared on this program have shown that consistently good performance can be achieved with propellants with flame temperatures from 5600°F to 6500°F. Increased motor pressure and increased propellant flame temperature increase the erosion rate of pyrolytic graphite more significantly than does increased oxidation potential of the propellant within the range studied. Motor tests of pyrolytic graphite produced by commercial vendors are in general agreement with data on our own coatings except that the incidence of mechanical failure has been higher with vendor-coated nozzles. Tests at other facilities also substantiate the erosion resistance of pyrolytic graphite coatings when mechenical failures are prevented.

Adequate design is a necessity to utilize the inherent capabilities of pyrolytic graphite. A segmented nozzle design has been adopted at Atlantic Research and has proved very useful. In the past large scale nozzle tests of pyrolytic graphite have been hampered by loss of coatings, but several successful tests do substantiate the serviceability of the material.

Scale-up efforts in this program included the successful test firing of two one-inch diameter nozzles under severe operating conditions and the design and preparation of a two-inch test nozzle. This work should be continued so that the orderly development of techniques to utilize the excellent properties of pyrolytic graphite can be achieved. Several firings with both one inch and two inch nozzles are recommended so that the consistent performance capabilities

of well-designed pyrolytic graphite nozzles can be proved. The successful completion of such a series of test firings would provide the assurance needed to approach full-scale nozzle design utilizing this exceptional nozzle material.

Commanding Officer
U. S. Army Weapons Command
Watervliet Arsenal
Watervliet, New York
Attn: Mr. F. Dashnaw (1)

Director
PLASTEC
Picatinny Arsenal
Dover, New Jersey (1)

Chief, Bureau of Naval Weapons
Department of the Navy
Room 2225, Munitions Building
Washington 25, D. C.
Attn: RMMP (1)

Department of the Navy
Office of Naval Research
Washington 25, D. C.
Attn: Code 423 (1)

Department of the Navy
Special Projects Office
Washington 25, D. C.
Attn: SP 271 (1)

Commander
U. S. Naval Ordnance Laboratory
White Oak, Silver Spring, Maryland
Attn: Code WM (1)

Commander
U. S. Naval Ordnance Test Station
China Lake, California
Attn: Technical Library Branch (1)

Commander
U. S. Naval Research Laboratory
Anacostia Station
Washington 25, D. C.
Attn: Mr. J. E. Srawley (1)

U. S. Air Force Directorate of Research & Development
Room 4D-313, The Pentagon
Washington 25, D. C.
Attn: Lt. Col. J. B. Shipp, Jr. (1)

Aeronautical Systems Division
Wright-Patterson Air Force Base, Ohio
Attn: H. Zoeller, ASRCEE-1-2 (2)
R. F. Klinger, ASRCEM-1 (2)

6593 Test Group (Development)
Edwards Air Force Base,
California
Attn: Solid Systems Div. DGSC (1)

AMC Aeronautical Systems Center
Wright-Patterson Air Force Base,
Ohio
Attn: Manufacturing & Materials
Technology Div, LMBMO (2)

U. S. Atomic Energy Commission
Office of Technical Information
Extension
P. O. Box 62
Oak Ridge, Tennessee (1)

National Aeronautics & Space Adm.
Washington 25, D. C.
Attn: Mr. B. G. Achhammer (1)
Mr. G. C. Deutsch (1)
Mr. R. V. Rhode (1)

George C. Marshall Space Flight
Center
Huntsville, Alabama
Attn: Dr. W. Lucas, M-S&M-M (1)
Mr. W. A. Wilson, M-ME-M (1)

Dr. L. Jaffe
Jet Propulsion Laboratory
California Institute of Technology
4800 Oak Grove Drive
Pasadena, California (1)

Aerojet-General Corporation
Post Office Box 1168
Sacramento, California
Attn: Librarian (1)

Aerojet-General Corporation
Post Office Box 1947
Sacramento, California
Attn: Mr. C. A. Fournier (1)

Aerojet-General Corporation
Azusa, California
Attn: Librarian (1)

Allison Division
General Motors Corporation
Indianapolis 6, Indiana
Attn: Mr. D. K. Hanink (1)

DISTRIBUTION LIST FOR
PYROLYTIC GRAPHITE FINAL REPORT

Office of the Director of Defense
Research & Engineering
Room 3D,1085, The Pentagon
Washington 25, D. C.
Attn: Mr. J. C. Barrett (1)

Armed Services Technical Information Agency
Arlington Hall Station
Arlington 12, Virginia
Attn: TIPDR (10)

Defense Metals Information Center
Battelle Memorial Institute
Columbus, Ohio (1)

Solid Propellant Information Agency
Applied Physics Laboratory
The Johns Hopkins University
Silver Spring, Maryland (3)

Commanding Officer
Army Research Office
Office Chief Research & Development
3045 Columbia Pike
Arlington, Virginia
Attn: Physical Sciences Division (2)

Commanding General
U. S. Army Materiel Command
Detachment I, Room 2502, Bldg. T-7
Washington 25, D. C.
Attn: AMCRD-RS-CM (1)

Commanding General
U. S. Army Electronics Command
Fort Monmouth, New Jersey
Attn: Mr. H. H. Kedesky (1)

Commanding General
U. S. Army Missile Command
Redstone Arsenal, Alabama
Attention: Documentation & Technical
Information Branch (2)
Mr. R. Fink, AMSMI-RKX (1)
Mr. E. J. Wheelahan, AMSMI-RSM (1)
Mr. R. E. Ely (1)
Mr. T. N. L. Pughe (1)
Mr. E. Fohrell (1)

Commanding General
U. S. Army Weapons Command
Rock Island, Illinois
Attn: Mr. B. Gerke (1)

Commanding General
U. S. Army Mobility Command
U. S. Army Tank-Automotive Center
Detroit 9, Michigan
Attn: Mr. S. Sobak (1)

Commanding General
U. S. Army Munitions Command
Dover, New Jersey (1)

Commanding Officer
Harry Diamond Laboratory
Washington 25, D. C.
Attn: Technical Library (4)

Commanding Officer
U. S. Army Chemical & Coating Lab.
Aberdeen Proving Ground, Maryland
Attn: Dr. C. Pickett (1)

Commanding Officer
U. S. Army Materials Research Office
Watertown Arsenal
Watertown 72, Massachusetts
Attn: OPT (1)
Technical Information Center (3)

Commanding Officer
U. S. Army Munitions Command
Frankford Arsenal
Philadelphia 37, Pennsylvania
Attn: Dr. H. Gisser, SMUFA-1330 (1)
Mr. H. Markus, SMUFA-1320 (1)
Mr. E. Roffman, SMUFA-1740 (1)

Commanding Officer
U. S. Army Munitions Command
Picatinny Arsenal
Dover, New Jersey
Attn: Mr. J. Matlack, Plastics &
Packaging Laboratory (3)
Mr. D. Stein (1)

Commanding Officer
U. S. Army Weapons Command
Rock Island Arsenal
Rock Island, Illinois
Attn: Laboratory (1)

Commanding Officer
U. S. Army Weapons Command
Springfield Armory
Springfield 1, Massachusetts
Attn: Research Materials Lab. (1)

ARDE-Portland, Inc.
100 Century Road
Paramus, New Jersey
Attn: Mr. R. Alper (1)

Boeing Company
Aerospace Division
Post Office Box 3707
Seattle 24, Washington
Attn: Mr. R. R. Barber, Library Unit Chief (1)

Curtiss-Wright Corporation
Wright Aeronautical Division
Wood-Ridge, New Jersey
Attn: Mr. A. M. Kettle, Technical Library (1)

Hercules Powder Company
Allegany Ballistics Laboratory
Post Office Box 210
Cumberland, Maryland
Attn: Dr. R. Steinberger (1)

Hughes Aircraft Company
Culver City, California
Attn: Librarian (1)

Narmco Research & Development
3540 Aero Court
San Diego 23, California
Attn: Technical Library (1)

Rohm & Haas Company
Redstone Arsenal Division
Redstone Arsenal, Alabama
Attn: Library (1)

Tapco Group
Thompson Ramo Wooldridge, Inc.
23555 Euclid Avenue
Cleveland 17, Ohio
Attn: Mr. W. J. Piper (1)

Thiokol Chemical Corporation
Redstone Division
Redstone Arsenal, Alabama
Attn: Library (1)

Chief, Bureau of Naval Weapons
Department of the Navy
Washington 25, D.C.
Attn: RRMA-22 (1)

Aeronautical Systems Division
Wright-Patterson Air Force Base,
Ohio
Attn: ASRCNC-2 (1)

Aeronautical Systems Division
Wright-Patterson Air Force Base,
Ohio
Attn: Mr. S. A. Mersol, ASRCMC (1)

Aeronutronics Division of
Ford Motor Company
Post Office Box 697
Newport Beach, California
Attn: Mr. Leon Green, Jr. (1)

Armour Research Foundation
10 West 55th Street
Chicago 16, Illinois
Attn: Dr. N. Parrikh (1)

AVCO Manufacturing Corporation
Research and Advanced Development
Division
201 Lowell Street
Wilmington, Massachusetts (1)

Beryllium Corporation
Reading, Pennsylvania
Attn: Mr. W. H. Santschi (1)

Carborundum Company
Research and Development Division
Niagara Falls, New York
Attn: Mr. Bruno Miccioli (1)

Clevite Corporation
Mechanical Research Division
540 East 105th Street
Cleveland 8, Ohio
Attn: Mr. G. Davis (1)

DATAC, Research Library A-52
The Martin Company
Post Office Box 179
Denver 1, Colorado (1)

Fansteel Metallurgical Corporation
North Chicago, Illinois
Attn: Mr. A. B. Michael (1)

General Electric Company
ANP Department
Research Information
Cincinnati, Ohio
Attn: Mr. H. E. Sauter (1)

General Electric Company
FPL Technical Information Center
Post Office Box 196
Cincinnati 15, Ohio (1)

General Telephone & Electronics Laboratories, Inc.
Bayside 60, New York
Attn: Mr. C. Wurms (1)

High Temperature Materials, Inc.
Technical Library
31 Antwerp Street
Brighton, Massachusetts (1)

A. D. Little, Inc.
Acorn Park
Cambridge 40, Massachusetts
Attn: Dr. R. Francis (1)

National Carbon Company
A Division of Union Carbide Corporation
Post Office Box 6116
Fostoria, Ohio
Attn: Library (2)

National Research Corporation
45 Industrial Place
Newton, Massachusetts
Attn: Document Control Section (1)

Raytheon Manufacturing Company
Research Division
Waltham 54, Massachusetts
Attn: Miss E. Weeks, Librarian (1)

Solar Aircraft Company
San Diego 12, California
Attn: Mr. N. B. Elsner (1)

Stauffer Chemical Company
1201 South 47th Street
Richmond 4, California
Attn: Mr. J. M. Fitzpatrick (1)

United Aircraft Corporation
The Library
400 Main Street
East Hartford 8, Connecticut
Attn: M. Lubin Thoren Kress (1)

United Nuclear Development
Corporation of America
5 New Street
White Plains, New York
Attn: Dr. Oppenheimer (1)

Value Engineering Company
Alexandria, Virginia
Attn: Mr. J. Huminik (1)

Westinghouse Electric Corporation
Materials Manufacturing Department
Blairsville, Pennsylvania
Attn: Mr. James McClure (1)

Georgia Institute of Technology
Engineering Experiment Station
Ceramics Branch
Atlanta, Georgia
Attn: Mr. J. D. Walton, Jr. (1)

Massachusetts Institute of
Technology
Cambridge, Massachusetts
Attn: Dr. J. Wulff (1)